Bioprotonics: Memories, Transistors, and pH Modulators

Yingxin Deng

A dissertation

submitted in partial fulfillment of the

requirements for the degree of

Doctor of Philosophy

University of Washington

2015

Reading Committee:

Marco Rolandi, Chair

Manjari P. Anantram

Peter Pauzauskie

Program Authorized to Offer Degree:

Materials Science and Engineering

University of Washington

Abstract

Bioprotonics: Memories, Transistors, and pH Modulators

Yingxin Deng

Chair of the Supervisory Committee:
Associate Professor Marco Rolandi
Department of Materials Science and Engineering

Protons (H^+) play an important role in controlling cell function and metabolic processes in biological systems. H^+ current affects a broad range of biological activities, from ATP synthesis in mitochondria[1] to neuron signaling in the brain.[2, 3] Being able to control H^+ transfer with artificial devices would provide new opportunities to study the effect of H^+ on biological functions. This understanding will be vital in the development of novel therapies and sensors based on proton flux. This thesis focuses on controlling H^+ transfer in biopolymers with artificial devices. I first study the dynamics of palladium hydride (PdH_x) as H^+ injecting contacts and its use in protonic conducting devices. Two terminal devices with PdH_x contacts display memory behavior. With PdH_x as contacts, a polysaccharide integrated field effect transistor measures and modulates the flow of H^+. By changing the gate voltage, this H^+ conducting channel can be turned on or off. In analogous to semiconductors, a proton semi-conductor model is developed to describe H^+ conduction. At last, I look at the applications of such H^+ conducting devices for pH modulation in solution.

TABLE OF CONTENTS

LIST OF FIGURES

ACKNOWLEDGEMENTS

I would like to express my sincere gratitude to Professor Marco Rolandi for letting me work in the bioprotonics field and being an encouraging advisor along the way. I benefit tremendously from his advice and enthusiasm for science. I would like to thank all the group members from Rolandi Research Group for assistance to my research and insightful discussions in the lab. It has been great fun working in a lab with a lot of friendship. Special thanks to Dr. Chao Zhong for his guidance when I first started my Ph.D., and the generosity of sharing his experience; to Dr. Takeo Miyake for the electrochemistry lessons and always being able to help. Before I met Erik Josberger, I thought electronic devices were rather boring. But after discussion with Erik, my attitude became positive, especially when we use electronic devices to study a different type of charge carrier. I would like to thank my committee members for taking their time out of their schedule to give me suggestions and critiques to help me improve: Dr. M.P. Anantram, Dr. Peter Pauzauskie, Dr. Dwayne Arola, and Dr. François Baneyx.

The work will not be done without our collaborators, Dr. M.P.Anantram and Anita Fadavi Rousdari (University of Waterloo, Electrical Engineering) for their help on device simulation; Dr. Brett Helms at the Molecular Foundary of the Lawrence Berkeley National Lab for the assistance on OH^--type protonic conductor synthesis; Dr. Róisín Owens at the Department of Bioelectronics of École des Mines de Saint-Étienne for the cell compatibility tests; Dr. Clara Santato and Dr. Julia Wünsche for their contributions on melanin proton conductivity study.

I would like to thank the University of Washington Royalty Research Fund and New Faculty Seed Funding, 3M Untenured Faculty Award for funding the polysaccharide bioprotonic field effect transistor work. I would like to thank National Science Foundation Career Award (DMR-1150630) for funding PdH_x-Nafion synaptic and memristive devices, OH^--type proton conductor synthesis, the complementary protonic devices, melanin proton conduction study. I would like to thank the University of Washington CGF award, Coulter Foundation Grant for funding the complementary protonic devices study. I would like to thank U.S. Department of Energy, Office of Science, Basic Energy Sciences (DE-SC0010441) for funding the protonic contacts depletion measurement and modeling, PdH_x formation in solution and enzyme logics.

And finally, to mom and dad for their love and being open-minded; to all my families and friends for being supportive all the time. This thesis could not be completed without you.

DEDICATION

Dedicated to the memories of my Grandfather 邓纪元 (1925-2014) and my Grandmother 何亚莉 (1926-2014)

Chapter 1. INTRODUCTION

1.1 Ion Flow in Biological Processes

Chaos theory describes the “butterfly effect”, where flap of a butterfly's wings in South America can affect the weather two continents away. This phrase is used to describe how small changes to a seemingly unrelated condition can affect large, complex systems. Our body is a multifunctional and intricate system, and the ion flow in and out of cell membranes are like the flapping wings of a butterfly. Ionic flow is usually trivially small, but it affects our body functions in tremendous ways. As I type my thesis after dinner, fingers are moving and the pancreas is producing insulin at the same time. Both the muscle contraction and hormone secretion are regulated by different ionic signals. When ion channels open in cell membranes, ions start to flow along the electrochemical gradient. The change of ion concentration sends out a signal to the cell, for example signaling the beta cells in the pancreas to release insulin and regulate metabolic processes.

Neurons are the most electrically excitable cells in our body, and neuron functions can affect our emotion, learning abilities, and memory formation.[4] Ion pumps located at the membranes control voltage gradients across the membranes. The ion pumps, combined with ion channels, generate intracellular and extracellular concentration differences of ions such as sodium, potassium, chloride, and calcium. The cross membrane voltage changes within the nerve cell build up until the cell sends a spike of electrical potential along the axon to the synapses, where the message is passed on to the next cell in the pathway. Researches have suggested that extracellular pH can have important effects on neuron function. In central and peripheral neurons, acid-sensing ion channels (ASICs) have emerged as key receptors for extracellular protons, and recent studies suggest diverse roles for these channels in the pathophysiology of pain, ischemic stroke and psychiatric disease.[2]

Aerobic respiration in mitochondria supplies energy in the form of ATP to fuel our daily activities. ATP is the principal molecule for storing and transferring energy in cells. The proton motive force (proposed by Mitchell in 1961), a proton gradient across membrane, powers ATP synthesis (Figure 1.1).[5] The energy released by the oxidation of food is used to pump protons

across a membrane, creating a proton reservoir on one side. The flow of protons through proteins embedded in this membrane powers the synthesis of ATP. Protons power respiration not only in mitochondria, but also in bacteria and archaea (Figure 1.1). Proton gradients are equally central to all forms of photosynthesis, as well as to bacterial motility (via flagellar motor) and homeostasis. Even fermenting bacteria, which do not need proton gradients to generate ATP, maintain the proton motive force, using ATP derived from fermentation to power proton pumping.[1, 6]

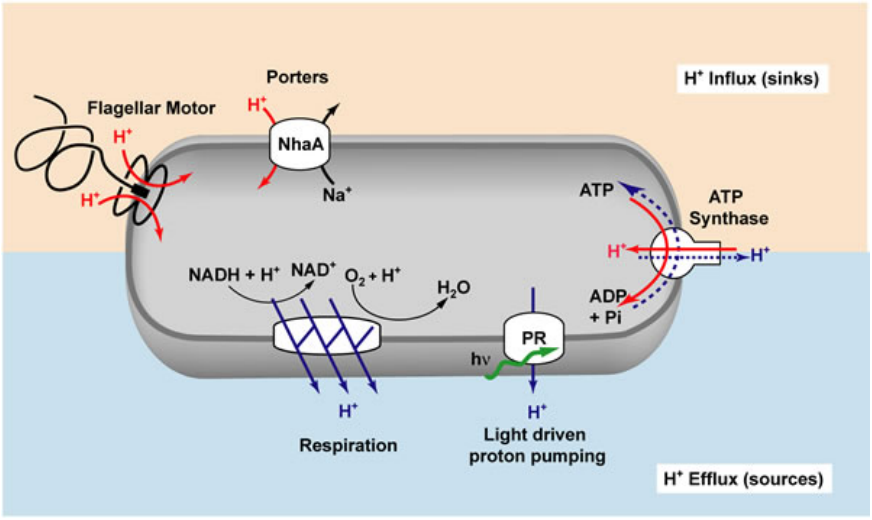

Figure 1.1. Proton flux in E.coli. This overview of transmembrane fluxes and proton pumping in E.coli cell carrying proteorhodopsin show respiration and light-driven proton pumping as sources of proton motive force that can power such functions as ATP synthesis and the rotation of the flagellar motor. Reproduced with permission from. [6] Copyright 2007, Proceedings of the National Academy of Sciences.

1.2 GROTTHUSS MECHANISM

In 1806, Grotthuss predicted H^+ transfer in water, even before the molecular structure of water was identified by Avogadro in 1811. He proposed that *oxygen and proton hop* (quoted from Grotthuss's original paper) to a dissociated water molecule.[7] This hopping process is now known as Grotthuss mechanism. A proton (H^+) enters the water file by forming a covalent bond with a water molecule to form a hydronium ion (H_3O^+). This H_3O^+ is transferred along hydrogen bonded water chains (proton wires) by exchanging the covalent bond on H_3O^+ with the hydrogen bond formed with a neighboring water molecule as shown in Figure 1.2 a. [8] The rate of H^+ hops within the water chains determines the charge transfer rate. The H^+ hopping process does not change the structure of the proton wire but leave the water chain in a polarized state. In order for the proton wires to transfer a second H^+, the wires have to turn 180° (Figure 1.2 a). Then the water chain will reorder by the transport of a Bjerrum D orientation defect (Figure 1.3a, c). The transfer process can support both hydronium (H_3O^+) ion and hydroxyl (OH^-) ion transfer along the chain. In the case of OH^- hopping (Figure 1.2 b), water molecule gives off a H^+ and forms a hydroxyl group, OH^-. Then, the hydroxyl group receives a H^+ from an adjacent water molecule. The negative OH^- thus travels along the proton wire to transport charge. A Bjerrum L orientation defect happens in the transport of an OH^- ion (Figure 1.3 b, d). With the ability to transfer both H^+ and OH^-, the protonic conductivity involves two different charge carriers similar to electrons and holes in semiconductors.[9] The sustained H^+ conductivity requires the transfer of H^+ and OH^- ions as well as Bjerrum D and L defects.

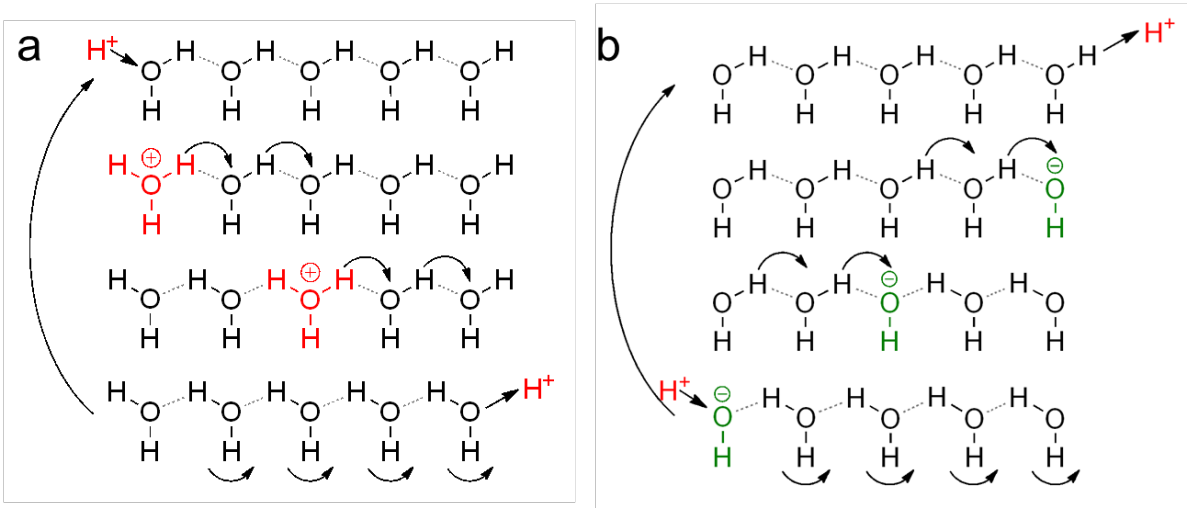

Figure 1.2. Grotthuss mechanism in water. Grotthuss mechanism for (a) H^+ conduction and (b) OH^- conduction along the hydrogen bonded water chain

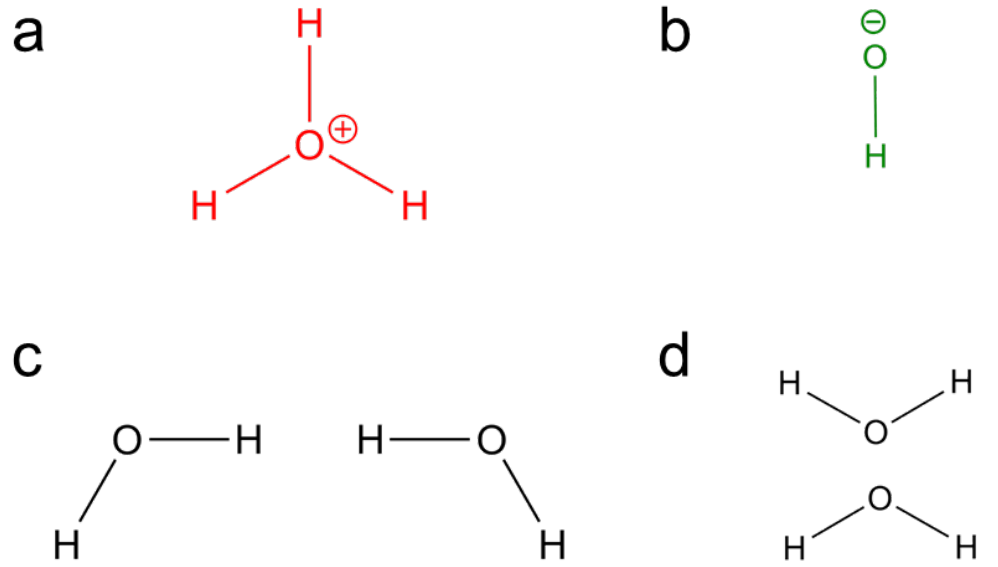

Figure 1.3. Potential defects in hydrogen bonded systems. a) Hydronium ion, b) Hydroxyl ion, c) Bjerrum D defect, d) Bjerrum L defect.

H^+ transfer has been intensively studied in water and ice. The reported value of H^+ mobility in water at 25 °C is 3.62 x 10^{-3} cm^2 V^{-1} s^{-1}, and 1.98 x 10^{-3} cm^2 V^{-1} s^{-1} for OH^-.[10] The transfer rate of H^+ is faster in ice due to the more ordered lattice structure of ice compared to water. The reported H^+ mobility value in ice (-10 °C) is 0.1 to 0.5 cm^2 V^{-1} s^{-1} and for OH- is $\leq$ 0.05 cm^2 V^{-1} s^{-1}.[10] As the existing of abundant water chains in biological systems, biomaterials transport H^+ as well. Collagen is a protein that consists of triple helices in the form of long rods. Those rods are packed in a regular lattice, leaving spaces or channels available for water. The water molecules form H bonds with the peptide groups. Ionic conductivity was measured in collagen and found to increase with hydration level of the material.[11] Another fibrous protein, keratin, from wool has demonstrated ionic conductivity when hydrated.[12] Keratin can form a H-bonded water network with amino acids groups on its side chains, and these groups contribute to H^+ current. Recently, the study of the gramicidin A (gA) proton pathway revealed more details about H^+ transport along water channels (Figure 1.4).[13] gA is an antibiotic and has a monovalent cation selective channel which excels at H^+ transport. The hydrophobic side of the channel is facing outside while the hydrophilic inside can accommodate a file of water molecules. Those H-bonded water molecules form the H^+ transfer pathway. When a single file of water molecules is confined in a hydrophobic channel with a diameter of 4.0 Å, the calculated proton transfer rate is seven-fold faster than in bulk water.[14] The overall speed of H^+ transfer through a transmembrane water file is rapid, and can occur in less than 500 ps in gA channels. Single-channel currents corresponding to more than 2 x 10^9 H^+/s have been reported.[14] Besides biology, the most widely used H^+ conductor is the synthetic polymer Nafion. Nafion, which is typically used as the proton exchange membrane (PEM) in fuel cell, is H^+ conducting and electron insulating. In a fuel cell, H^+ generated from hydrogen oxidation at the anode travels through PEM and combines with oxygen at the cathode to produce water, while electrons flow through the outside circuit as electricity. Nafion has an inverted micelle structure where the hydrophilic sulfonate groups are facing inside the micelles and leave the hydrophobic Teflon backbone facing outside (Figure 1.5). In between the micelles are narrow canals. The narrow channels limit the ion transfer through the micelles in Nafion. When the material is hydrated, canals swell, hence lowering the energy barrier for ion transfer. At high hydration level, Nafion is an efficient H^+ conductor with reported H^+ conductivity of 0.08 S/cm.[15-17]

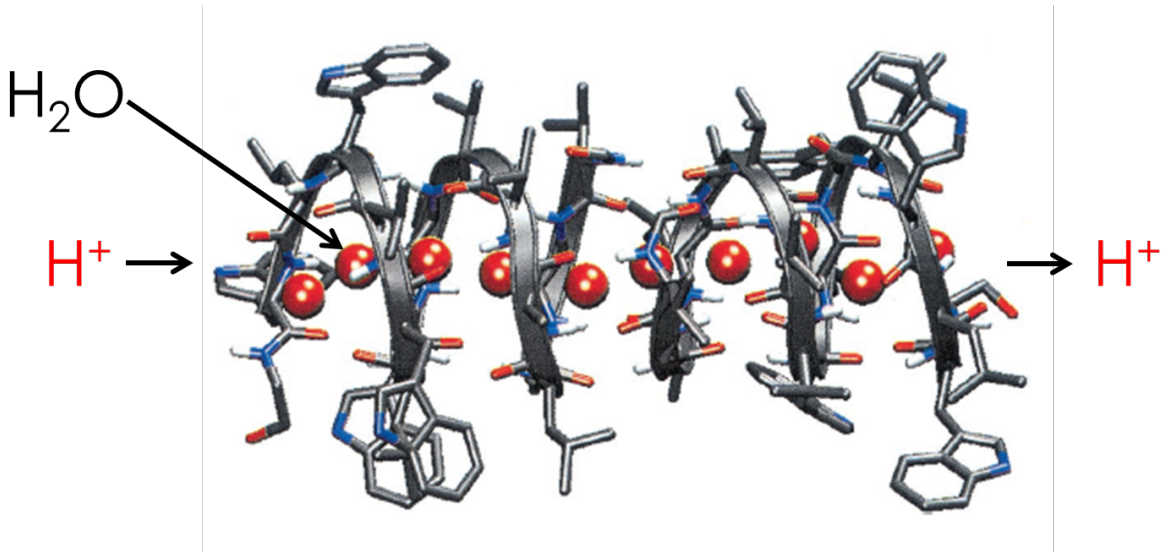

Figure 1.4. Gramicidine A proton channel. Reproduced with permission from[13]. Copyright 2002, Biophysical Journal.

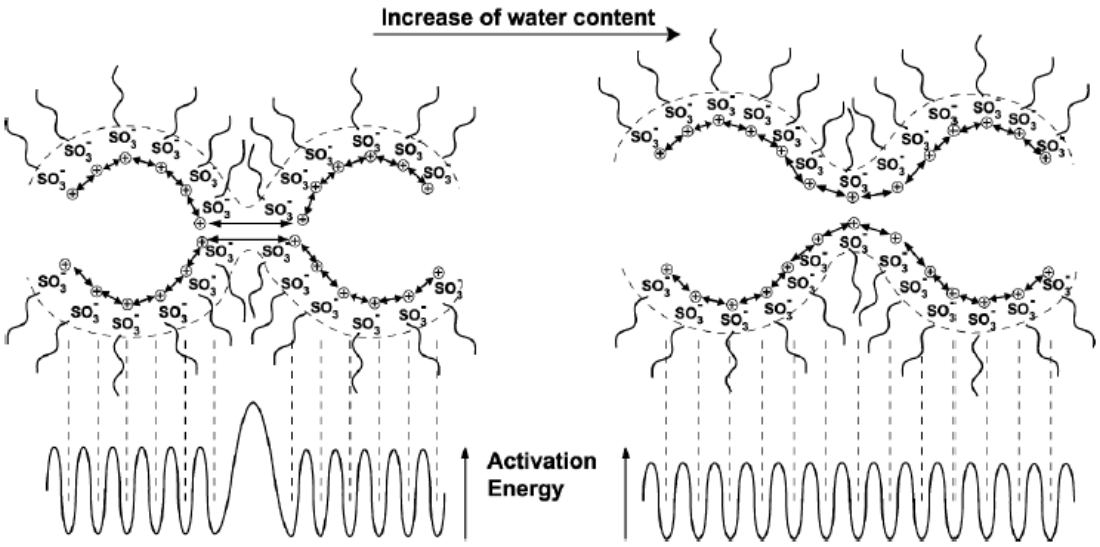

Figure 1.5. Internal structures of Nafion. Hydration of the Nafion opens up the narrow pathway in between the micelles, lowering the activation energy for H^+ transfer. Reproduced with permission from [17]. Copyright 1990, Journal of Electroanalytical Chemistry.

1.3 BIOELECTRONICS

The combination of living systems with artificial devices has fascinated mankind from the time of early science fictions to emerging efforts to create a man-made robot. More than two centuries ago, when Luigi Galvani (1737-1798) and his assistant were dissecting a frog near a static electricity generator, the steel scalpel was accidentally in touch with the frog leg. They noticed that the dead frog leg twitched. Noting the simultaneous spark, Galvani started a series of measurements showing muscle contraction. The notion of "animal electricity" discovered by Galvani led to the study of electrophysiology. Following the exciting route, Walter Hess (1881-1973) placed a needle electrode in a cat's brain to send electrical current, which lead to the development of current therapeutic use of deep brain stimulation, for example, for Parkinson's disease treatment (approximately 30,000 people worldwide now have electrodes implanted in their brains to treat this condition).[18] The history of science is often a story of new devices and new technologies. With the recent flourishing of nanotechnology, miniaturization of electronic devices is able to detect or stimulate biological functions down to a single cell level, reveling the information unable to measure with traditional micro sized equipment.

1D nanomaterials, such as carbon nanotubes and silicon nanowires, have been used to construct electronic devices that incorporate functional biological membrane proteins, channels, and pumps (Figure 1.6).[19, 20] Gramicidin and bacteriorhodopsin have been integrated with carbon nanotubes[21] and field effect transistors (FETs) [22] to develop biosensors with increased functionality. These devices control the protein functionality, read the signals sensed by these proteins, and mimic the cellular transport processes. FETs with incorporated silicon nanowires are able to perform single-molecule detection[23] and high-sensitivity recording in physiological conditions[24, 25]. Nonvolatile or programmable memoristors[26] and synaptic transistors[27] can mimic neuron activities and brain functions in neuromorphic computing.

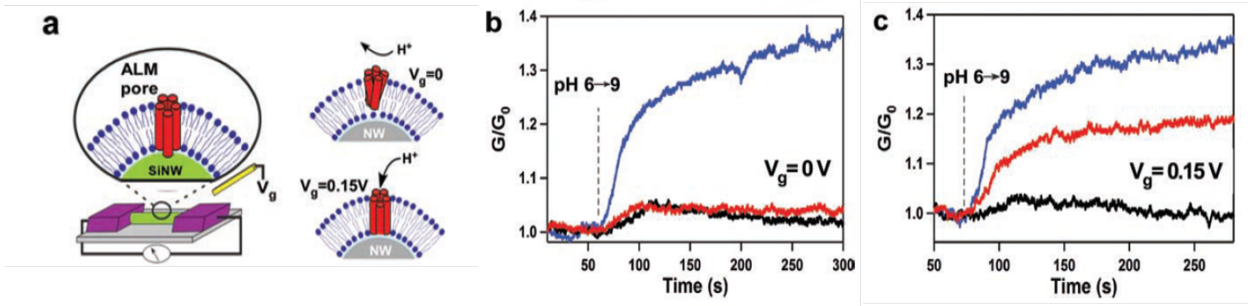

Figure 1.6. Bionanoelectronic device with voltage-gated ion channels. (a) (Left) Schematic of a nanowire transistor in which a Si nanowire (green) is connected to the source and drain electrodes (purple). The nanowire is covered with a lipid bilayer that incorporates ALM protein pores (red). (Right) ALM conformation in the membrane at $V_g = 0$ (closed state) and $V_g = 0.15$ (open state). (b) Time traces of normalized conductance of the Si nanowire device held at gate bias of 0 V recorded as the solution was changed from pH = 6 to pH = 9 for the uncoated nanowire (blue trace), coated nanowire (black trace), and the coated nanowire device incorporating the ALM pores (red trace). c) Time traces of a similar experiment recorded at gate bias of 0.15 V. Vertical dashed lines indicate the time when the pH of the fluid cell input stream started to switch from the lower to the higher value. Reproduced with permission from Advanced Materials, Copyright 2011.[19]

Organic electronics differ from conventional electronic materials in that they conduct both electrons and ions. Another difference is in their chemical structure, which more closely resembles biological systems (proteins, polymers) than rigid inorganic metals and silicon.[19, 28] For these reasons, organic electronics are increasingly being applied in biological settings. Organic electronic devices are designed to allow control over the processing, transport and delivery of ionic and molecular signals. Organic field effect transistors (OFETs) are used for biomolecule sensing[29] and recording brain activity with high signal-to-noise ratio in the brain;[30] electronic ion pumps can control ion transfer and delivery;[31, 32] ion bipolar junction transistors (IBJTs) (Figure 1.7)[33] in integrated ionic circuits would be one approach to route and dispense complex chemical signal patterns. Organic electrochemical transistors (OECTs) combine the benefits of biocompatibility, easy fabrication, and flexibility, and provide a sensitive way to detect minute ionic currents in electrolytes. OECTs are coupled with different biorecognition elements, such as the barrier tissue[34] and redox enzymes[35] as sensing platforms for biological ion flow.

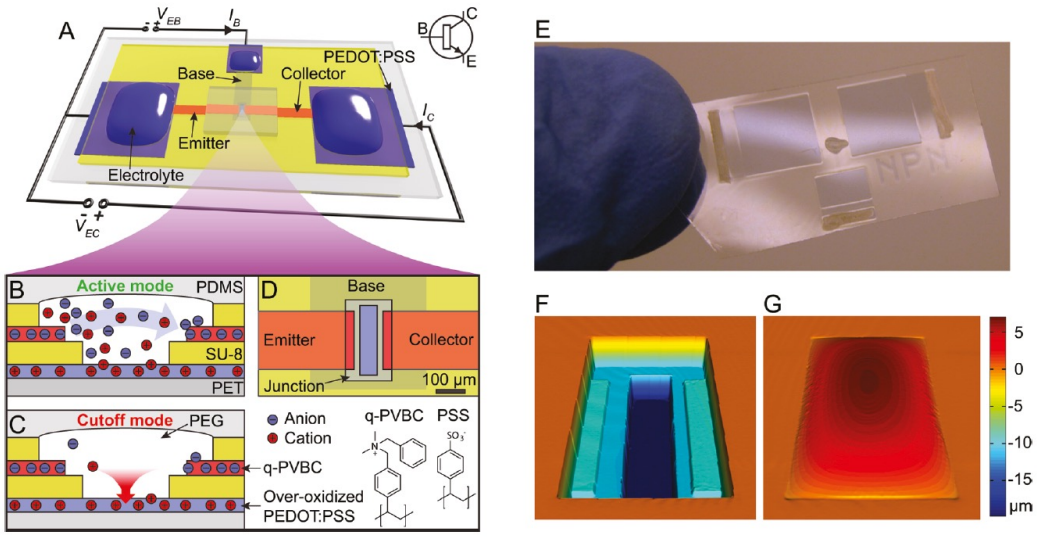

Figure 1.7. Conducting polymer based npn-IBJT. (A) The emitter and collector are separated from the base by a neutral polymer electrolyte. Conductive PEDOT:PSS electrodes covered by electrolytes inject/extract ions to/from the terminals of the transistor. (B) In the active mode the base supplies the junction with cations. (C) In the cutoff mode the base depletes the junction of mobile cations. (D) The junction is formed by an opening in the SU-8 insulation layers which is filled with a polymer electrolyte. The distance between the emitter and collector is 100 µm. (E) Photograph of the fabricated device with painted silver contacts. The three PEDOT:PSS electrodes and the PDMS encapsulation are visible. (F) Measured topographies of the junction before and (G) after the PEG electrolyte was applied. Reproduced with permission from Journal of the American Chemical Society, Copyright 2011.[36]

1.4 THIS THESIS

Biological ion flux is important for a number of different processes including enzyme activity, neuron functionality, and regulating metabolic processes. Following the exciting routes of bioelectronics research, I study the control of ion flux, especially protons, with electronic devices. We call this research bioprotonics. I demonstrate that bioprotonic devices can modulate proton transfer in biopolymers and in solution. Such artificial devices are an ideal means for interfacing with biological systems.

Chapter II explores the mechanisms of H^+ conducting contacts. Palladium hydride (PdH_x) is the protods (H^+ transparent contacts) in bioprotonic devices. This chapter discusses the dynamics of PdH_x. Palladium (Pd) absorbs hydrogen gas (H_2) and forms PdH_x. When applied to a bias, PdH_x injects a H^+ into the proton conducting channel and an electron goes to the outside circuit for current measurement. The drift current density in proton conducting channel affects hydrogen (H) diffusion in PdH_x. Hence we develop a drift-diffusion model to study the contact behavior. PdHx protodes also show memory behavior when reversing the applied bias.

Chapter III demonstrates that a field effect transistor (FET) integrated with H^+ conducting polysaccharide nanofibers can control proton current. The H^+ concentration in the polysaccharide channel can be turned on or off by controlling the electrical voltage applied at the gate contact. H^+ mobility in the channel $\mu_{lin}^{H+} = (5.3 \pm 0.5)10^{-3}\,\mathrm{cm^2V^{-1}s^{-1}}$, is in agreement with the reported H^+ mobility in diluted acid. Simulations as a semiconductor type FET (performed with Dr. M.P. Anantram, UW Dept. of Electrical Engineering), but substituting the hole mobility with proton mobility, agrees with the device behavior.

Following the same rationale of H^+-type FET, I demonstrate a OH^--type FET, regulating the proton hole (OH^-) concentration in the channel in Chapter IV. I use gradual channel approximation to look at how the gate voltage would affect the source drain current. To describe the device behavior, we develop a proton semiconductor model. H^+ and OH^- are charge carriers in proton conducting materials, similar as electrons and holes in semiconductors. The model is based on a semiconductor band structure, consisting of a quasi proton valence band and a quasi proton conduction band. We discuss the band gap or the activation energy, and the protochemical potential.

Chapter V investigates the H^+ transfer between the protodes and solution. H^+ concentration in solution defines the pH values, which is a frequent regulator for biological functionalities. An electrochemical setup controls the H^+ transfer via the voltage applied between the working electrode and the reference electrode. Substituting the conventional platinum (Pt) counter electrode to a high capacitance electrode used in electric double layer capacitor (EDLC) can store the H^+ concentration change in the solution, thus changing the pH. The pH modulator can control the light emitting firefly bioluminescent reactions.

Chapter 2. PALLADIUM HYDRIDE PROTODES

Abstract

Experiments on palladium hydride (PdH_x) elucidate its function as H^+ injecting contacts. The dynamics and memory behavior of PdH_x protodes are analyzed from the two-terminal measurement with maleic chitosan and Nafion. The drift current density in proton conducting channel affects hydrogen (H) diffusion in PdH_x. A high drift current density in the channel would deplete the contact, while at a low current density in the channel PdH_x acts as a H^+ injecting contact. Hence we develop a drift-diffusion model to study the contact behavior. PdH_x protodes also show memory behavior when reversing the applied bias.

2.1 INTRODUCTION

Electrical devices operate with electrons through metallic conductors. To measure proton current, metal electrodes must then be in contact with the proton conductor for a continuous current to pass. This brings one of the basic problems with any ion conduction process, for electron-ion exchange must occur at the interface in order to maintain a current flow. One solution is to use electrodes that can be the sources or sinks of protons. Palladium metal, by virtue of its ability to absorb and transmit hydrogen as well as to conduct electronically, provides the most convenient proton conducting electrodes "protodes"[10, 37] to act as a proton source. Pd is used industrially as a catalyst for, e.g. hydrogenation reactions and exhausts gas cleaning, and is unique among the metals because it combines a high activity for hydrogen splitting with a high solubility for hydrogen in the bulk. Palladium (Pd) forms PdH_x by absorbing hydrogen gas (H_2) from the atmosphere[38] or by being made the cathode in an electrochemical cell[39, 40]. When applied to a bias, PdH_x injects a H^+ into the proton conducting channel and an electron collected by the lead completes the outside circuit for current measurement.

This chapter is presented in a similar form as it was published in Advanced Materials (Josberger E. E., Deng Y. et al., Two-terminal protonic devices with synaptic-like short-term depression and device memory, Advanced Materials, 26, 29, 4986-4990, 2014, http://onlinelibrary.wiley.com/doi/10.1002/adma.201400320/abstract). Reproduced with permission from Advanced Materials.

2.2 PALLADIUM HYDRIDE

The Palladium (Pd) - Hydrogen (H) system is one of the most widely and thoroughly investigated bulk metal - hydrogen systems studied to date. Pd soaks up hydrogen like a sponge. The ability of Pd to absorb up to 900 times its own volume of H at room temperature has led to its application in hydrogenation reactions and as a hydrogen storage material.[41, 42] Pd can reversibly absorb hydrogen gas and form palladium hydride PdH_x. Depending on different hydrogen gas partial pressure in the atmosphere the value of x varies from 0 to 0.69.[43] Pd is characterized by a face-centered cubic (FCC) structure, which has two types of interstitial sites, octahedral and tetrahedral. H atoms absorbed from gas phase by Pd are stored at the octahedral sites. It is assumed that H diffuses in a perfect Pd crystal by jumping from one octahedral site to another. The diffusion process will be perturbed by the defects in the metal structure, thus H will be trapped.[39] At room temperature, palladium hydrides may contain two crystalline phases, α and β (Figure 2.1). Pure α phase exists at $x < 0.017$ whereas pure β phase is realized for $x > 0.58$; intermediate x values correspond to α-β mixtures. The diffusion coefficient of H varies in different phases.[43] PdH can also be formed in solution using electrochemical methods, which is described in details in the references.[40, 44]

Palladium also has been used as a protonic conductor. In 1986, Morgan developed a proton injecting technique for the measurement of hydration dependent protonic conductivity.[45] In his experiment, a hydrogen saturated Pd electrode infused H^+ into the H-bonded water chain in cyclodextrin and contributed to the current. The protonic current increased with the material hydration level. When a voltage is applied, PdH gives off a hydrogen ion (H^+) and an electron following the reaction: $PdH \rightarrow Pd + H^+ + e^-$.[9] H^+ thus hops from the PdH_x contact into H-bonded proton wires in the polymer and conducts following the Grotthuss mechanism. A higher hydration level denotes a higher density of water network in the material, contributing to higher protonic current. In this way, PdH_x can be used as an H^+ injecting contact (Figure 2.2).

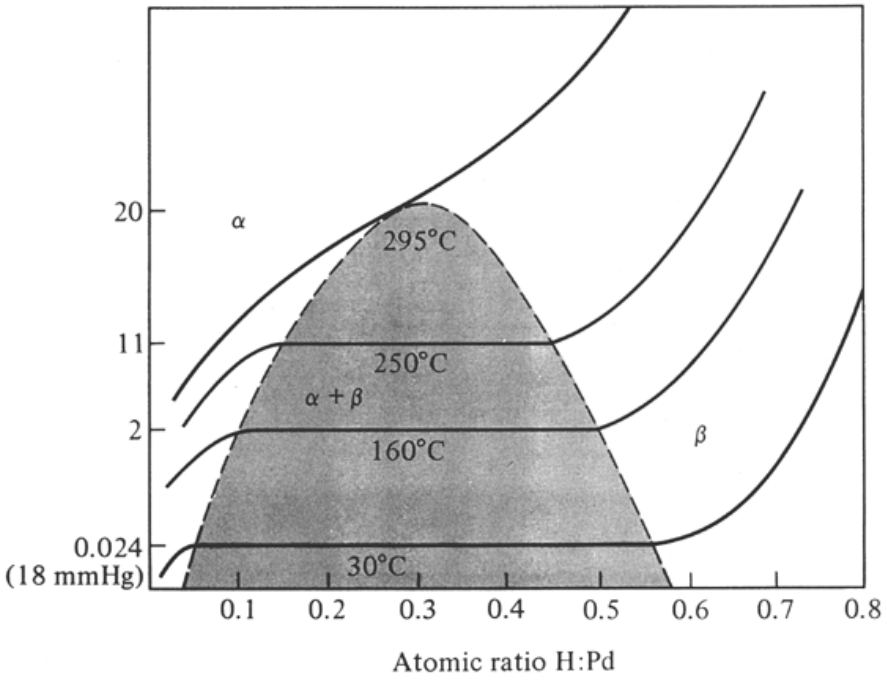

Figure 2.1. Absorption relationships in the palladium-hydrogen system. Reproduced with permission from.[46] Copyright 1977, Platinum Metals Review.

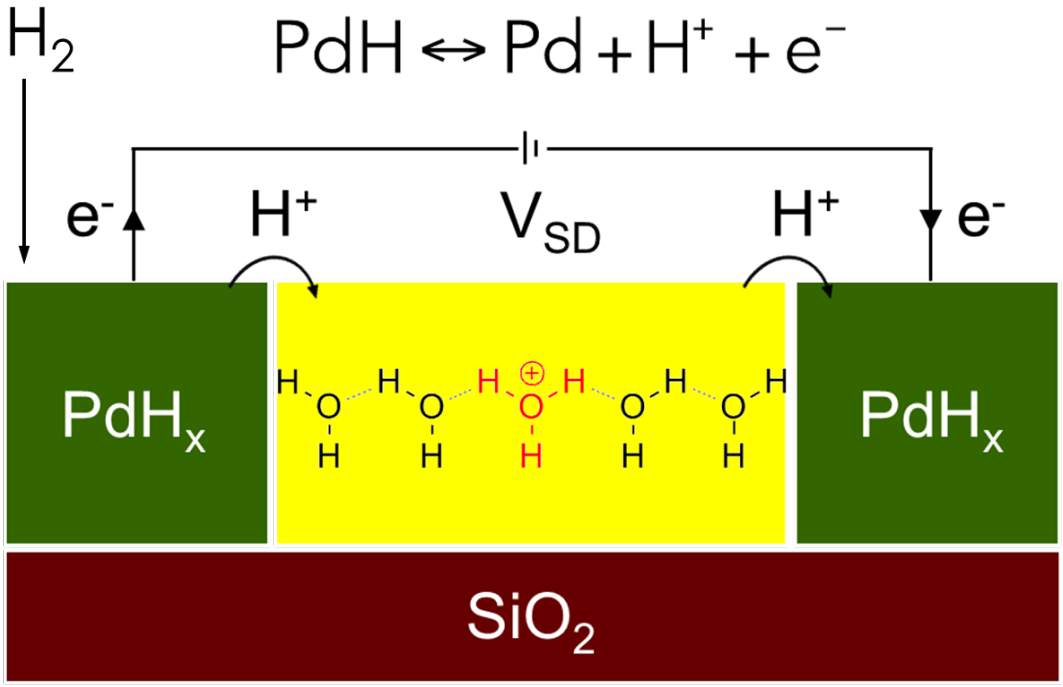

Figure 2.2. Two terminal protonic device with PdH_x contacts.

2.3 H^+ Injection from Protodes

To prove the H^+ injecting ability of PdH contacts, H^+ conductivity of a polysaccharide derivative was measured with PdH. The H^+ conducting biopolymer is maleic chitosan (poly(β-(1,4)-N-Maleoyl-D-glucosamine) and is synthesized in the lab.[47] Maleic chitosan is a polysaccharide chitin derivative. It is water soluble, biocompatible, and nontoxic (Figure 2.3 a, b).[47] Maleic chitosan is cell friendly and biocompatible, which makes it a good candidate to interface with biological systems. The carboxyl groups in maleic chitosan can donate H^+ ions and form H bonds with surrounding water molecules easily. The H-bonded network is crucial for protonic conductivity (Figure 2.3 c). According to the Grotthuss mechanism, H^+ can transfer in maleic chitosan water network by hopping from one H-bond to another. The moving protons can transfer from one PdH_x contact to the other, giving rise to the protonic current.

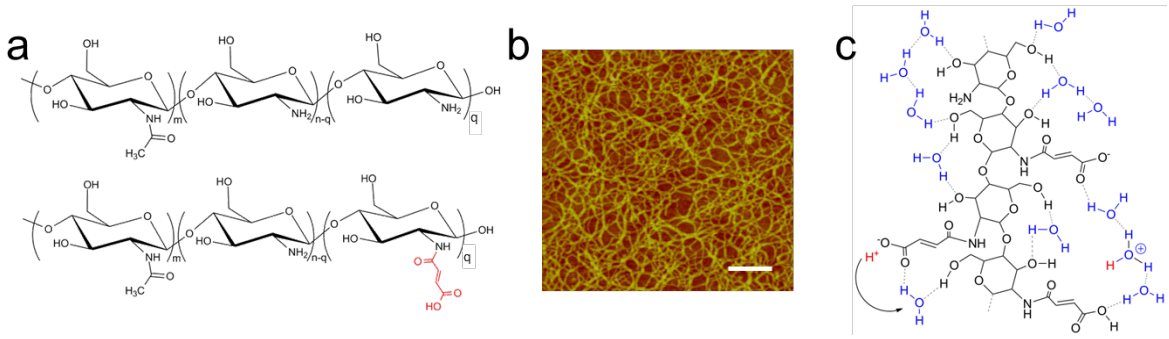

Figure 2.3. Proton conducting maleic chitosan. (a) Molecular structure of chitin and maleic chitosan molecule. (b) Atomic force microscope of maleic chitosan nanofibers on a silicon substrate. Scale bar is 200 nm. (c) The intra and intermolecular hydrogen bonds between four-monomer segment of maleic chitosan and surrounding water molecules. The maleic group donates a H^+ to the H bond network and forms a H_3O^+.

To demonstrate the formation of the H-bonded network with the increased hydration level of the material, the measurement was first carried out in a two-terminal device (Figure 2.4 a). Two $1cm^2$ Pd contacts sandwiched a maleic chitosan film. 5 mL 3.0% (w/v) maleic chitosan water solution were dropped in a clean Teflon plate. After drying for 5 hours, a thin film formed and was carefully peeled off from the Teflon plate. Copper wires were connected at the back of the Pd contacts. The humidity level was adjusted by flowing N_2 gas through a water bubbler into the sealed humidity chamber. The humidity dependence test was done in 5% hydrogen gas. The increased current showed the influence of humidity level in protonic conductance (Figure 2.4 b). Large amount of water contribute to the H-bonded network formation.

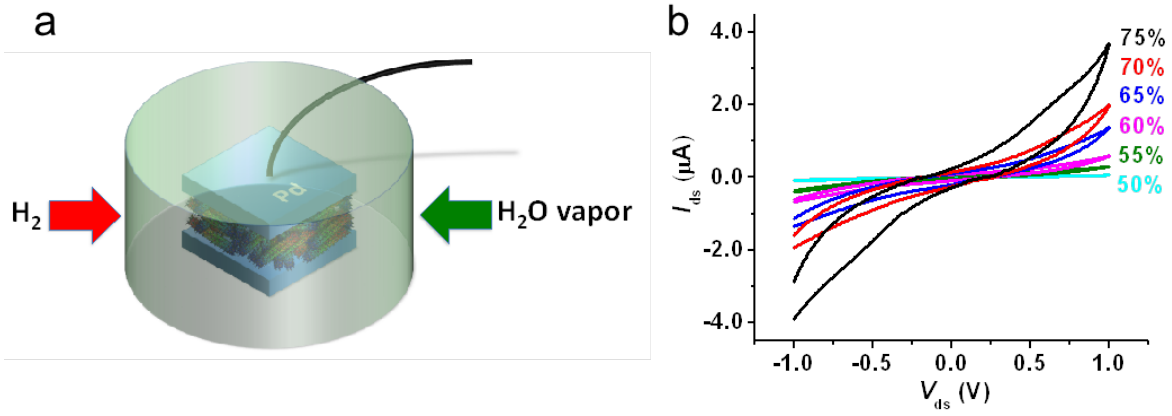

Figure 2.4. Relative humidity dependence of maleic chitosan proton conductivity. (a) Schematic of a two-terminal device. H_2 gas and H_2O vapor were flowed into the testing chamber. (b) The humidity dependence of maleic chitosan. The H^+ current increases with rising humidity.

The second bulk film test was to prove the formation of H^+ injecting PdH_x contacts under exposure of H_2. The test was done with the same experimental settings but with a H_2 depleted Pd contact and a gold (Au) contact (Figure 2.5). Humidity was kept at 75% RH with the flow of N_2 gas through water bubbler. The control experiments with Pd or Au (with H_2 gas) contacts are almost 20 times lower compared to PdH_x. Both Pd and Au are known as good electronic conductors. But without the formation of PdH_x, only electronic current can be measured. H^+ injected from PdH_x contacts increases the total conductivity of the material by allowing the flow of H^+ between the contacts. This proves that the PdH_x contacts are H^+ transparent and the protonic current, rather than the electronic current, is the major contribution to the conductivity.

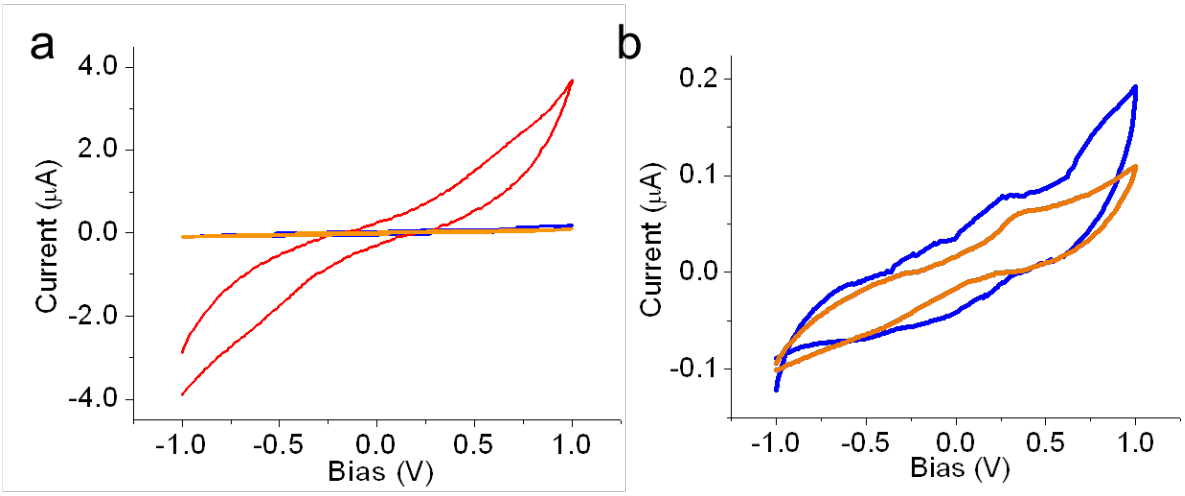

Figure 2.5. Comparison of maleic chitosan proton conductivity with Au, Pd, and PdH_x contacts. (a), (b) Maleic chitosan measured at 75% RH with Au contacts (orange), H_2 depleted Pd contacts in N_2 (blue), PdH_x contact in 5% H_2 (red). Note: b, is magnified curve from a. Contact area is 1 cm^2; film thickness is ~300 μm each.

2.4 Dynamics of Protodes

The measurement with maleic chitosan and PdH_x in the experiment demonstrated that PdH_x is H^+ transparent. A drift-diffusion process drives the H^+ transfer from one PdH_x contact to the other.[48, 49] In particular, the PdH_x contacts display a depletion behavior for high current densities. Erik Josberger developed a simple one-dimensional physical model (Figure 2.6) to illustrate the dynamics of PdH_x contacts. In this model the diffusion flux (J_H) of hydrogen inside the PdH_x contact follows Fick's first law of diffusion and conservation of mass. For this simple model, we neglect any exchange of hydrogen between the PdH_x and the surrounding H_2 atmosphere. Assuming continuity across the PdH_x and H^+ conductor boundary, we postulate that the current of H^+ in the H^+ conducting channel (I_{H+}) is equal to J_H in the last PdH_x cell in contact with the H^+ conductor times the charge of a proton (e) and the contact area of the device (A). Therefore, the hydrogen diffusion in the PdH_x is driven by the induced electric drift of H^+ from the contact-conductor interface and along the H^+ conducting channel, in a fashion similar to the transfer of H^+ to an acidic water solution in the palladium hydrogen reversible electrode.[48] This model does not include any trap states,[48] or the accurate 2D device geometry, which likely affect the I_{H+} characteristics in the experimental protonic devices. As expected, a hydrogen-depleted region of Pd grows with time in the source contact and results in a smaller I_{H+} when the device is eventually turned from the ON to the OFF state.

$$J_H = D_H \frac{dn_H}{dx} \qquad I_{H+} = AeJ_H$$

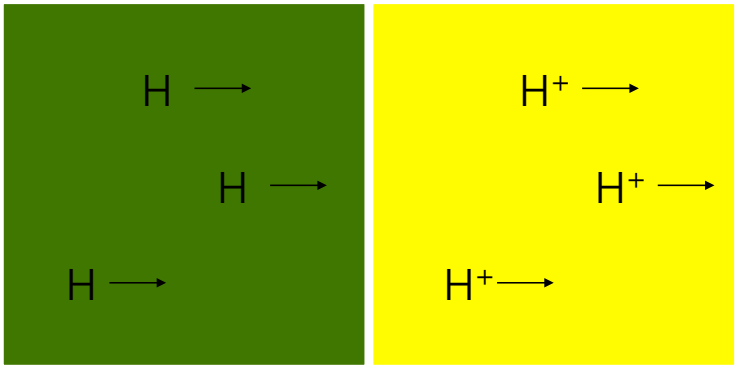

Figure 2.6. Schematic of the drift-diffusion model

Nafion is a proton-conducting and electron insulating polymer widely used as proton exchange membrane in fuel cells, with a proton conductivity of 0.078 S cm^{-1}.[16] Nafion is a more efficient proton conductor, which enables a higher current density in the channel. A Pd-Nafion two terminal device (Figure 2.7 a) was built to investigate the depletion process in PdH_x contacts. The devices were fabricated on p-type Si (Addison Engineering, B-doped, ρ = 0.001 ohm cm-1) with thermally grown silicon oxide (100 nm). Standard photolithography is used to define the metal contacts. Pd (thickness from 1nm to 30 nm) with a 15 nm Cr adhesion layer is deposited via e-beam evaporation (Balzers PLS 500). To ensure consistency, contacts are kept at a 100 nm total thickness by adding Au between the Cr and Pd layers as needed. SU-8 is used to confine the Nafion covered area. 2 μL Nafion 117 solution (5% concentration) from Sigma Aldrich is drop-cast on top of the patterned silicon wafer and the solution is dried in a fume hood.

PdH_x contacts inject and drain H^+ into and from the proton-conducting Nafion.[9, 45, 50, 51] For each H^+ injected into the Nafion, an excess electron is collected by the leads, which complete the circuit. An applied voltage (V_{SD}) causes an H^+ current (I_{SD}) to flow between source and drain contacts in the protonic device (Figure 2.7 b). This current depletes H from the PdH source where in direct contact with the Nafion.[9, 45, 50, 51] This depletion creates a H concentration gradient in the PdH_x and a subsequent diffusion flux inside the contact. For low current densities, the diffusion flux in the PdH_x, the absorption of H from the H_2 atmosphere, and I_{SD} balance out and the PdH_x contacts effectively function as protodes - the protonic equivalent of electrodes.[9, 45, 50, 51] For higher current densities, as in the Nafion channel, a region of the source fully depletes of H to form Pd. Pd can no longer inject H^+ in the Nafion and I_{SD} decays as a function of time. As a result, a V_{SD} pulse produces a spike in I_{SD} as the contact depletes (Figure 2.7 b). This type of transient behavior has previously been observed in PdH_x reversible electrodes in contact with an acidic solution.[48] After waiting a determined period of time (300 s) allows the source to replenish H from the atmosphere and a later V_{SD} pulse results in an I_{SD} spike of the same magnitude as the first one. To corroborate this picture, we fabricate PdH_x contacts of varying thicknesses (Figure 2.7 c). Thinner contacts deplete faster than the thicker ones due to overall lower amount of H available in the PdH_x to be injected in the Nafion as H^+. A similar effect is also observed by loading contacts of same thickness with less H by exposing them to a lower H_2 concentration in the atmosphere (Figure 2.7 d). Thicker contacts (30 nm and 10 nm) result in comparable device I_{SD}, while 5 nm PdH_x contacts show lower I_{SD} most likely due to reduced

contact quality. Contacts with an equivalent thickness of Au, but no PdH_x (0 nm), result in little or no current as expected. Au is an excellent electronic contact, but cannot inject H^+ into the Nafion. Nafion is a proton conductor and an electronic insulator. A limited source contact area between the PdH_x and the Nafion (Figure 2.7 e) affords switching speeds of 25 ms with an on-off ratio of approximately 100. The switching speed depends on V_{SD}. For a Nafion channel with fixed resistance, a larger V_{SD} results in higher I_{SD} and faster contact depletion (t_D). In these devices, V_{SD} is limited to ≤ 1.3 V to avoid water electrolysis. For a given contact thickness, we assume that the PdH_x source contains a fixed amount of H and the contact is fully depleted when an equivalent amount of charge flows in the device channel as H^+. To confirm this observation, the total amount of charge (Q) flowing across the Nafion channel during an I_{SD} spike is calculated as

$$Q = \int_{t=0}^{t=t_D} I_{SD}\, dt \quad (1.1)$$

Integrating I_{SD} as a function of time gives the total number of H^+ ions that flow across the channel, and therefore the total number of H atoms stored in the contact. The measured Q is constant as a function of V_{SD} and increases with PdH_x thickness (Figure 2.7 f). The conservation of charge as calculated in equation (1.1) means that a larger I_{SD} results in a shorter t_D. Device miniaturization with thinner contacts and shorter contact separation may lead to faster devices with shorter t_D.

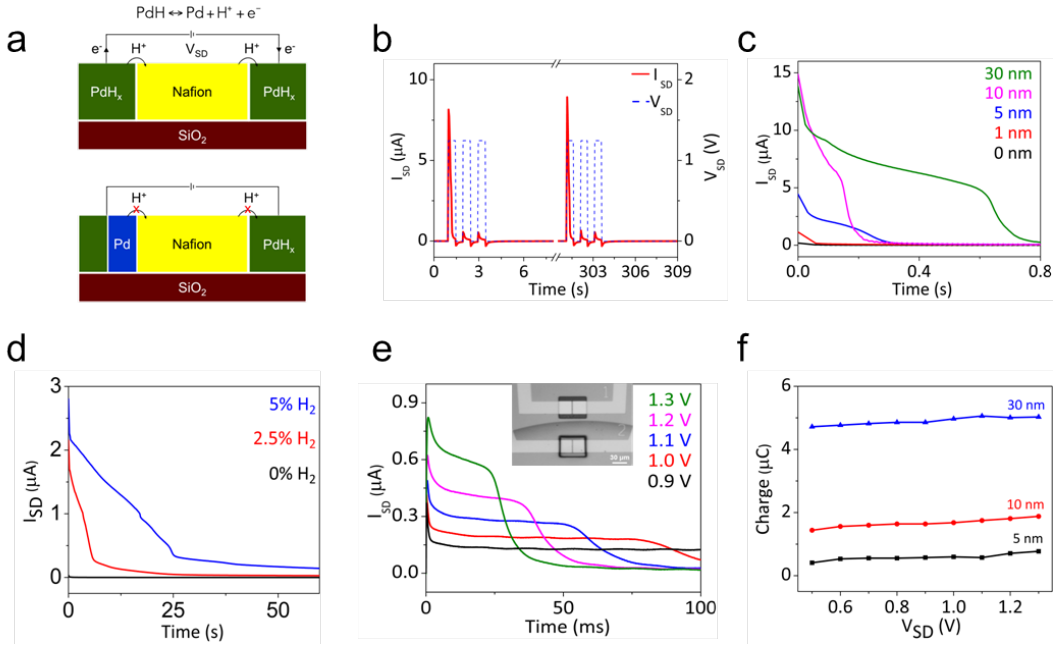

Figure 2.7. Dynamics of PdH_x contact. (a) Schematics of PdH_x-Nafion device. V_{SD} is applied across two PdH_x contacts. A H^+ current (I_{SD}) flows from the source to the drain through H^+ conducting Nafion. I_{SD} depletes the PdH_x to form Pd (not proton conducting). (b) I_{SD} as a function of time for a protonic device 30 μm wide by 500 μm long (c) Current spike behavior (V_{SD}= 1 V) as a function of PdH_x contact thickness. (d) Time scale of micro-device depletion dependence on atmospheric H_2 concentration. (e) I_{SD} dependence on V_{SD} and I_{SD} at t = 0s. Contact is 10 nm thick PdH_x. Insert: Microscope image of a PdH_x -Nafion device. Lithographically patterned source and drain contacts 30 μm wide are separated by a 1μm gap. (f) Total charge flux required for complete depletion of PdH_x source contact as a function of V_{SD} and Pd thickness.

2.5 Memory Behavior of Protodes

With these protonic devices, a two-terminal with reconfigurable "ON" and "OFF" states device was built to demonstrate memory behavior of PdH_x contacts (Figure 2.8). Pd (50 nm) is evaporated on glass slides with 5 mm contacts defined by shadow masking with tape. A porous cellulose membrane (VWR Tissue Wipe) immersed in the Nafion solution is sandwiched between the two Pd contacts. The cellulose membrane prevents short circuit and improves the connection. Measurements are performed with a semiconductor parameter analyzer (Agilent 4155C). A Rigol DG4062 function generator is used to create a pulse sequence and sinusoidal inputs. Device testing is performed on a Signatone H-100 probe station in a controlled atmosphere of 5% H2, 95% N2, at 75% relative humidity (RH).

A protonic memory in the ON state (Figure 2.8 a) conducts I_{SD} with a small V_{SD} applied. A positive V_{SD}= 1.5 V turns the protonic memory OFF (Figure 2.8 b). A reverse V_{SD}= -1.5 V injects H^+ back into the source to reform PdH_x and RESETs the memory to the ON state (Figure 2.8 c). To monitor this process, a sandwich device on transparent glass supports was fabricated and the source in the different memory states under an optical microscope was imaged (Figure 2.8 d, e, f, g).[52] Upon H absorption from the H_2 atmosphere, the source changes color from metallic Pd to white PdH_x (Figure 2.8 d). A positive V_{SD} pulse depletes the PdH_x of hydrogen, and the PdH_x returns to metallic Pd as seen in the OFF state device (Figure 2.8 e). When the device is RESET, H is loaded back into the source as H^+ from the Nafion channel to form white PdH_x (Figure 2.8 f). Memory cycling is demonstrated from the I_{SD} output of a protonic device (Figure 2.8 h) with the same structure as the one described in Figure 13. The magnitude and the time duration of the I_{SD} spike resulting from the RESET V_{SD} pulse are the same as the magnitude and the time duration of the I_{SD} spike for the ON-OFF V_{SD} pulse. This signifies that a fixed

amount of H is shuttled between the source and drain in the form of an H^+ current in the Nafion (I_{SD}). It is conceivable that the ON-OFF cycle does not increase the concentration of H in the post-synaptic contact to x > 0.6. The equilibrium pressure of H_2 increases exponentially when x is above 0.6.[53] Therefore, it is likely that additional hydrogen added to a contact that already has x=0.6 rapidly diffuses into the atmosphere instead of increasing the hydrogen loading of the PdH_x. Cycling the protonic device by applying a 2 Hz, 1 V sine wave to V_{SD} confirms the device characteristics with a clear hysteresis between the ON and OFF states (Figure 2.8 i). I_s is the same in either direction, which is similar to unipolar resistive switching.[54] Cycling is performed 22 times indicating reasonable reproducibility. Starting at V_{SD} = 0 V and increasing V_{SD}, the device is in the ON state and turns OFF at up to V_{SD} = 1V, at which point the source is fully depleted of H and is no longer capable of injecting H^+ into the Nafion channel. The device stays OFF for $V_{SD} > 0$ until the polarity of V_{SD} is reversed. A device in the OFF state for $V_{SD} > 0$ V is in the ON state for $V_{SD} < 0$ V because the PdH source is not depleted of H and is capable of injecting H^+ into the Nafion channel. A $V_{SD} < 0$ V depletes the source of H and the device eventually turns OFF for V_{SD} = -1 V. At the same time, a $V_{SD} < 0$ V moves H^+ back into the source, which is replenished of H and the device is in the ON state for $V_{SD} > 0$ V. The state of these devices is governed by the amount of charge flux that has gone through the device, specifically the amount of H^+ that is shuttled back and forth in the Nafion channel. As such, these protonic devices may have similar characteristics to memristors with the charge flux being the state variable.[55, 56] However, in these protonic devices the hysteresis loop is not pinched with zero crossing, which is a characteristic of memristors. Further work is necessary to develop a full analytical description of the device characteristics.

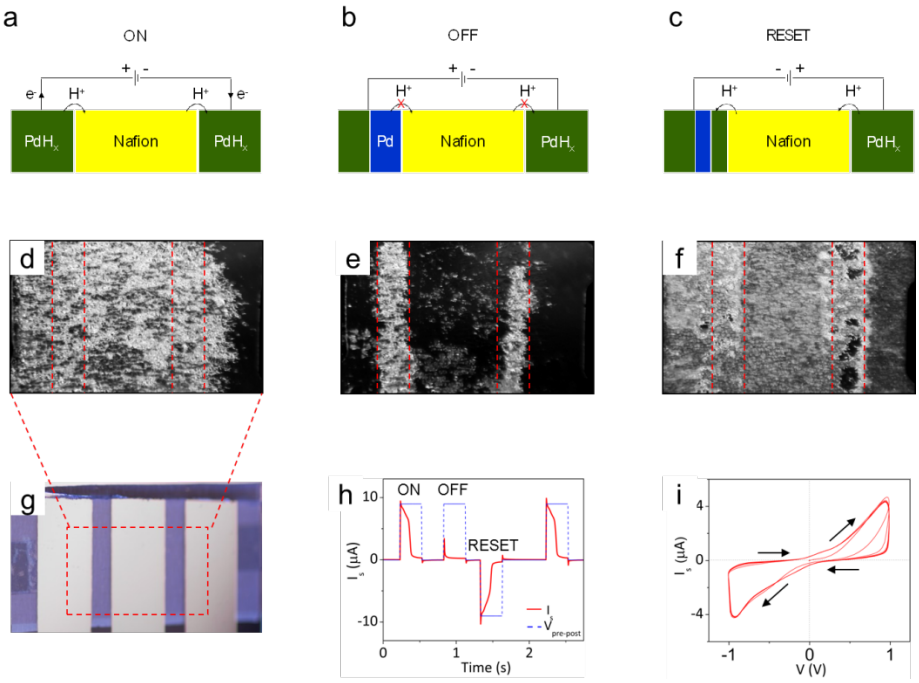

Figure 2.8. Memory behavior of PdH_x contact. (a), (b), (c) Schematic side views of protonic devices showing proton depletion and reset in the source contact. (a) ON state. (b) OFF state after a V_{SD} pulse and resulting I_{SD} spike depletes the PdH_x source of H to form Pd. (c) RESET. A negative V_{SD} injects H^+ back into the source to form PdH_x. (d), (e), (f), (g) Optical images of a PdH_x source in a sandwich device fabricated on glass. Lighter areas are PdH_x and darker areas are Pd. (d) $V_{SD} = 0$ V. (e) $V_{SD} = 1.25$ V. (f) $V_{SD} = -1.25$ V. (h) Demonstration of ON and OFF switching in an analogous micro device. Three positive SET pulses ($V_{SD} = 1.25$ V, 0.25 s) and a negative RESET pulse ($V_{SD} = -1.25$ V, 0.25 s) were applied. (i) I-V curve for a micro device, showing the hysteresis in the PdH_x -Nafion system.

2.6 CONCLUSION

I demonstrated that the proton injection ability of PdH_x contacts. First I studied the dynamics of PdH_x contacts. Together with Erik, we used a simple drift-diffusion model to study the transfer of H^+ in the device. The model provided insights in the spatial dependence of the H concentration (x) in the PdH_x source contact at different time points. Contact depletion measurements of PdH_x indicate that PdH_x function as H^+ injecting contacts at a low current density (J_H). J_H increased as applied voltage (V_{SD}). In this case, a high J_H will turn the device off, thus halting the H^+ injection from PdH_x. A negative V_{SD} can reverse the H depletion in PdH_x contacts. This depletion process is an example of a memory behavior.

Chapter 3. H^+-TYPE FIELD EFFECT TRANSISTOR

Abstract

After demonstrating PdH_x works properly as a H^+ injecting contact at low current density in the channel, Chapter 3 presents a field effect transistor (FET) integrated with PdH_x contacts and a H^+ conducting maleic chitosan channel. The H^+ FET can conduct and control proton flow. The H^+ concentration in the polysaccharide channel can be turned on or off by controlling the electrical voltage applied at the gate contact. The protons move along the hydrated maleic chitosan hydrogen-bond network with a mobility of $\sim 4.9\times10^{-3}$ cm^2 V^{-1} s^{-1}.

3.1 INTRODUCTION

In living systems, electrical signals are communicated and processed by modulating ionic[57] and protonic currents.[58] In contrast, the development of computing has mainly focused on devices that control electronic currents such as vacuum tubes, solid-state field-effect transistors (FET), and nanoscale molecular structures.[59-62] Few examples of protonic-based devices exist, and include an ice FET working with AC current,[63] and a water bipolar junction transistor.[64]

At the nanoscale, ionic (and protonic) conductivity has attracted increasing interest with the advent of resistive ionic memories,[54] memristors,[65] synaptic transistors,[66] and nanofluidics.[67, 68] In hybrid bionanodevices, biological multifunctionality has been added to carbon nanotubes[69] or silicon nanowires[70] with transmembrane proton conductive proteins. Bionanoelectronic devices[19] that can control the current of ions and protons, a more appropriate language than electrons in nature,[71] are uniquely positioned. In this regard, nanofluidics devices are particularly attractive. However, these require microscopic liquid reservoirs, and current control at physiological concentration is limited to difficult-to-fabricate nanometer channels.[68]

Recently, conducting polymer ion bipolar junction transistor devices have been demonstrated.[72, 73] These exploit ion selective membranes as contacts to extract and deliver ions (Na^+, K^+, Ca^{2+}) and neurotransmitters in solution. To further this exciting route, biocompatible field-effect devices with H^+ selective solid-state contacts would allow exclusive interfacing with biological proton-conducting channels.

This chapter is presented in a similar form as it was published in Nature Communications (Zhong C., Deng Y. et al., A polysaccharide bioprotonic field-effect transistor, Nature Communications, 2, 476, 2011, http://www.nature.com/ncomms/journal/v2/n9/full/ncomms1489.html). Reproduced with permission from Nature Communications.

3.2 H^+ Field Effect Transistor

Electrical characterization was then done on a three terminal device with a source, drain and gate contact (Figure 3.1). The testing device was fabricated using standard photolithography (as described in 2.3). Pd contacts are insulated from the silicon back gate by 100 nm thick silicon dioxide layer. Purified maleic chitosan was dissolved in DI water to form 0.002% (w/v) solution. 2 μL maleic chitosan aqueous solution was dropped on the device to form a good connection between drain and source. The solution was dried under N_2 flow.

A humidity dependence test on the small-scale device showed increased current with increasing humidity. The voltage V_{ds} (0 - 1 V) between drain and source was applied during the test and the current I_{ds} were recorded. Since the H+ charge carriers in the device are positively charged, a negative gate voltage increases the current, and vice versa. The results show the gating effect of the protonic field effect transistor (Figure 3.1 b).

A simple model was developed to describe the H^+-FET. When the channel length is the same, I_{ds} is proportional to V_{ds}. The conductivity (σ) of the channel can be calculated based on the conductivity equation $\sigma = e\, n^{H+}\, \mu^{H+}$ (e = proton charge, n^{H+} = number of free protons per unit volume, and μ^{H+} = proton mobility). Proton mobility will stay the same when we apply different V_{gs}. Different I_{ds} values in the experiment results were from the effective H+ concentration change in the channel. When a negative V_{gs} is applied, excess protons will be drawn onto the channel. They will contribute to the conductivity as an increase in the n_{H+} (higher I_{ds}). The increase can be estimated by a factor of $(-V_{gs}C_g/et)$ (t = channel thickness, C_g = capacitance per unit area) (Figure 3.1 d).[50] At the same time, a decrease in n_{H+} (lower I_{ds}) is expected for a positive V_{gs} (Figure 3.1 c). The derivation of H^+ mobility and concentration will be discussed in details in Chapter **Error! Reference source not found.**.

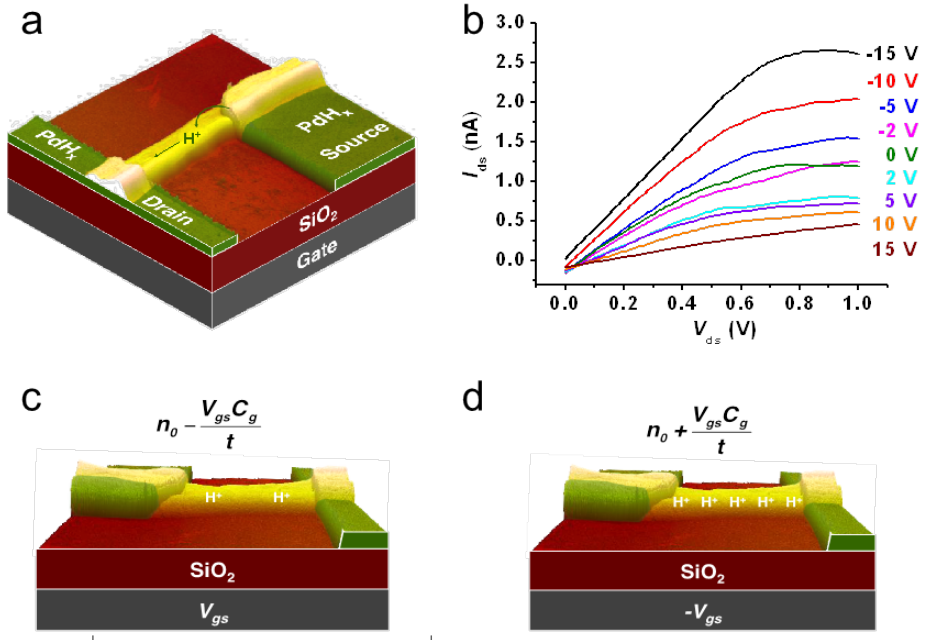

Figure 3.1. H^+-FET. (a) Schematic of H^+-FET. Maleic chitosan nanofibers bridged over the PdH_x contacts on a back gated transistor. PdH_x contacts are 10 µm wide, with 8.6 µm spacing. The insulating SiO_2 layer is 100nm thick. Maleic chitosan thin film is 3.5 µm wide, 8.6 µm long and 80 nm thick. (b) Plot of I_{ds} as a function of V_{ds} for different V_{gs} at 75% RH with the flow of H_2 gas. (c), (d) Schematics showing the charge carriers (H^+) concentration in maleic chitosan films when applying (c) positive and (d) negative gate voltage.

In collaboration with Anita Fadavi Rousdari from Electrical Engineering Department at the University of Waterloo and Prof. M. P. Anantram from Electrical Engineering Department at UW, simulation with the H^+-FET has been done. We produced 2D plots of proton density n^{H+} at different V_{gs} (Figure 3.2) by solving drift diffusion and Poisson equation in a semiconductor device simulator, where the hole mobility is replaced by proton mobility. The simulation results demonstrate higher proton concentration at negative V_{gs} and lower proton density at positive V_{gs}.

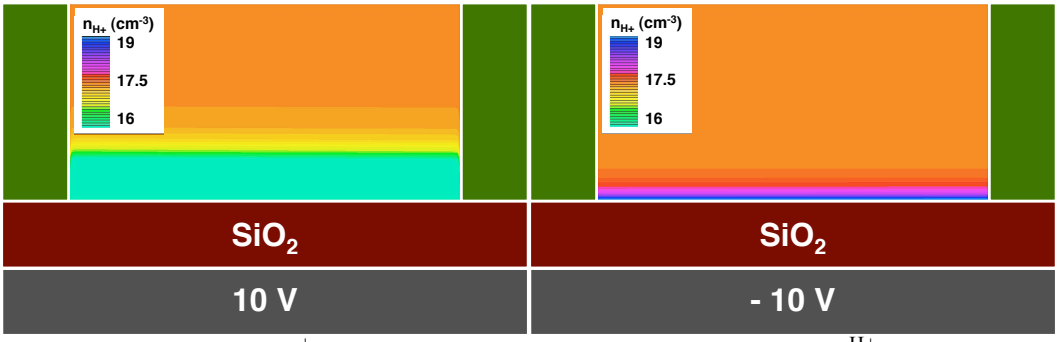

Figure 3.2. Simulaton of H^+-FET . Two-dimensional plots of device n^{H+} (log scale in cm^{-3}) as a function of V_{gs} (V_{ds} = 0.3 V)

3.3 CHARGE CARRIER CONCENTRATION ESTIMATE

An intuitive way to calculate the charge carrier concentration in protonic conductors might be to start from their chemical properties -that is, use the pK_a values of maleic chitosan functional groups to calculate the dissociated number of H^+. I first calculated the H^+ concentration in maleic chitosan. Here, an infinite dilution approximation was used to estimate maleic chitosan pK_a to calculate the H^+ concentration. The reported pK_a of carboxylmethyl chitosan ($-CH_2COOH$) is 3.4.[74] The maleoyl group (-COCH=CHCOOH) in maleic chitosan is a relatively stronger electron-withdrawing group compared with carboxylmethyl group, and thus making maleic chitosan a stronger acid with a relatively lower pK_a. Therefore, the pK_a value of 3.2 for maleic chitosan was used in the calculation.

In order to calculate the proton concentration, we first derive the concentration of carboxyl functional groups. The hydration level for maleic chitosan at 75% is 20.2 ± 1.3 wt%. Here we use 20 wt%. The degree of substitution (DS) of maleic chitosan=0.85. The average molecular weight for each repeating unit for maleic chitosan = 250.6

The carboxyl group concentration C (COOH) can be calculated by the following equation:

$C(COOH) = 0.85 \times C(\text{repeat unit})$

$= 0.85 \times n(\text{repeat unit})/V_{Total}$

$= 0.85 \times n(\text{repeat unit})/[V(H_2O) + V(\text{maleic chitosan})]$

$=0.85 \times (0.8/250.6)/ [0.2/\rho(H_2O) + 0.8/\rho(\text{maleic chitosan})]$

Because $\rho(H_2O)$ =1.0 g/cm3, ρ (maleic chitosan) = 1.4 g/cm^3 (based on the density of chitin=1.425 g/cm^3)

We obtain C (COOH) = 0.35*104 mol/m^3

The free protons can be considered to mainly come from dissociation of carboxyl groups on the polysaccharide molecules.

The initial concentration of carboxyl group is A_0, and after dissociation the concentration becomes (A_0- A)

	$RCOOH \leftrightarrow RCOO^-$	+	H^+
	A_0	0	0
After dissociation:	A_0-A	A	A

$pK_a = - \log 10 K_a$

$= - \log 10 ([RCOO^-] [H^+]/[RCOOH])$

$= - \log 10$

$= - \log 10 [A^2/(A_0 - A)]$

A0 = 3.5 mol/L, $pK_a = 3.2$, then we obtain A = 10 mol/L = 2.8×10^{19} cm^{-3}.

Note:

C (H_2O): Concentration of water molecules in the system

C (COOH): Concentration of carboxyl molecules in the system

N (H_2O): Total amount of water molecules in the system (in moles)

N (COOH): Total amount of carboxyl molecules in the system (in moles)

V_{Total}: The total volume of the system

V (H_2O): the volume of water molecules

V (maleic chitosan): the volume of maleic chitosan molecules

The H^+ concentration value from this pK_a calculation is 2.8×10^{19} cm^{-3}, 30 times different from the value calculated from the device 8.0×10^{17} cm^{-3} (estimate from device data is described in details in Chapter **Error! Reference source not found.**). The disagreement between the charge carrier density estimated from maleic acid dissociation and the charge carrier density calculated from the device data is not surprising. First because the pK_a value is defined for infinite diluted solution and we used the infinite dilution approximation in our calculation. This disagreement indicates that using the infinite dilution approximation for acid dissociation in this system is not appropriate. The infinite dilution approximation assumes the acid to be in water at pH 7, which is not affected by the additional protons donated by the acid. In our system, the resulting ionic strength is approximately 1mM. Additionally, the pK_a of acidic groups is affected by the dielectric permittivity of the medium with a shift to higher pK_a for lower dielectric constant.[75] The dielectric permittivity of water is 79 and we estimate the dielectric permittivity of the maleic chitosan to be approximately 10. When these factors are taken into account, the estimate charge carrier density is in closer qualitative agreement with the charge carrier density derived from the device data. [51]

It is difficult to clearly define pH in these types of biopolymer devices[76] and at the present moment it is not possible to quantitatively revise the estimate for n_{H+}^{0} from acid base dissociation. Nonetheless, the conductivity of chitin without maleic acid groups is reported in Chapter 4.2 to be significantly smaller than the conductivity of maleic chitosan for V_g=0. The dramatically lower conductivity of chitin confirms that the H^+ in the maleic chitosan channel is from dissociation of the maleic acid.

3.4 CONCLUSION

I demonstrated H^+ conduction in polysaccharide nanofibers. H^+ transparent PdH_x contacts measure H^+ current. The H-bonded water network is essential for H^+ conduction. H^+ dissociated from the acid group in maleic chitosan side chain transfers along the H-bonded network following the Grotthuss mechanism. A voltage to the gate contact can modulate the H^+ transfer, so the protonic device can turn on or off.

Chapter 4. COMPLEMENTARY PROTONIC DEVICES

Abstract

Proton conduction is essential in biological systems. In these systems, H^+ hop along chains of hydrogen bonds between water molecules and hydrophilic residues, the proton wires. These wires also support the transport of OH^- as proton holes. Discriminating between H^+ and OH^- transport has been elusive. Here, H^+ and OH^- transport is achieved in polysaccharide based proton wires and devices. A H^+-type and OH^--type junction with rectifying behavior and H^+-type and OH^--type complementary field effect transistors are demonstrated. We describe these devices with a model that relates H^+ and OH^- to electron and hole transport in semiconductors. These biocompatible protonic devices open exciting opportunities in bioelectronics for measurement and control of proton driven physiological functions. In turn, the model developed for these devices may provide additional insights into proton conduction in biological systems.

4.1 INTRODUCTION

Progress in bioelectronics now includes devices that mimic biological functionality and interface with biological systems.[19, 77] Memristors simulate synapses for neuromorphic computing.[78] Silicon nanowires record and stimulate single cell potential.[79] Gramicidin and bacteriorhodopsin are integrated with carbon nanotubes,[21] silicon nanowires,[70] and organic field effect transistors[22] to develop biosensors with increased functionality. Ionic[72] and mixed conductivity in biological[76] and organic polymers[28] are used to record and stimulate physiological functions, and assembled into logic circuits.[33] I have previously investigated H^+-FETs with polysaccharides that effectively mimic proton wires in ion channels.[50] Here, I demonstrate proton-conducting devices with polysaccharide supported proton wires that are designed to preferentially conduct either H^+ or OH^-, as proton holes. We explain the conductivity in these devices with a model for proton semi conductivity proposed in 1958 by Eigen and de Maeyer.[10] I demonstrate a H^+ OH^- rectifying junction and H^+-type and OH^--type complementary FETs. With gate control of the current, these FETs unequivocally discriminate between H^+ and OH^- conductivity and indeed confirm that proton wires support conduction of OH^- as a proton hole.

This chapter is presented in a similar form as it was published in Scientific Reports (Nature) (Deng Y. et al., H^+-type and OH^--type biological protonic semiconductors and complementary devices, Scientific Reports, 3, 2481, 2013, http://www.nature.com/srep/2013/131003/srep02481/full/srep02481.html). Reproduced with permission from Scientific Reports.

4.2 Protonic Semiconductor Model and H^+-/OH^-- Doping

As mentioned in 1.2, the sustained protonic conductivity requires the movement of H^+ and OH^- ions as well as Bjerrum D and L defect. The transport process needs energy, which makes protonic conductivity a thermally activated process. Previous studies of H^+ movement in water have reported that the activation energy for H^+ transport in water is about 0.86 molar eV.[10] This behavior of H^+ is similar to the charge carrier in electronic semiconductors. Eigen and de Maeyer first proposed a "protonic semiconductor" in 1958 "with an intrinsic (thermal) distribution of the charge carriers (protons) between a 'valence' band (H-bonded H_2O) and a 'conduction' band (excess protons fluctuating in H bonds)".[10] Here, a proton quasi-band model has been built and discussed (Figure 4.1 a, b). H^+ has the same contribution as electrons in semiconductors, and acid groups can be seen as H^+ donors. OH^- ions are like proton holes, and base groups can be treated as H^+ acceptors. Two kinds of energies are needed for proton transfer. The first is the activation energy. A neutral proton wire is not conductive unless energy is contributed to create a H^+ and OH^- pair (Figure 4.1 c, d). The energy is defined as band gap energy E_{gap}. The proton wire becomes conductive by H^+ hopping from the H^+ valence band (H-bonded H_2O) to the empty H^+ conduction band (excess protons fluctuating in H bonds). The other kind of energy required for H^+ to move is hopping energy, as depicted as energy wells in Figure 16 b. The hopping energy is smaller than E_{gap}. The energy can be calculated based on the Gibbs-Helmholtz equation, $E_{gap}=-k_BTlnK_w$, where K_w is the water dissociation constant = 10^{-14} at RT. E_{gap} is about 0.83 eV for a neutral proton wire. The value is similar to the activation energy measured for proton conducting biopolymers.[11, 12]

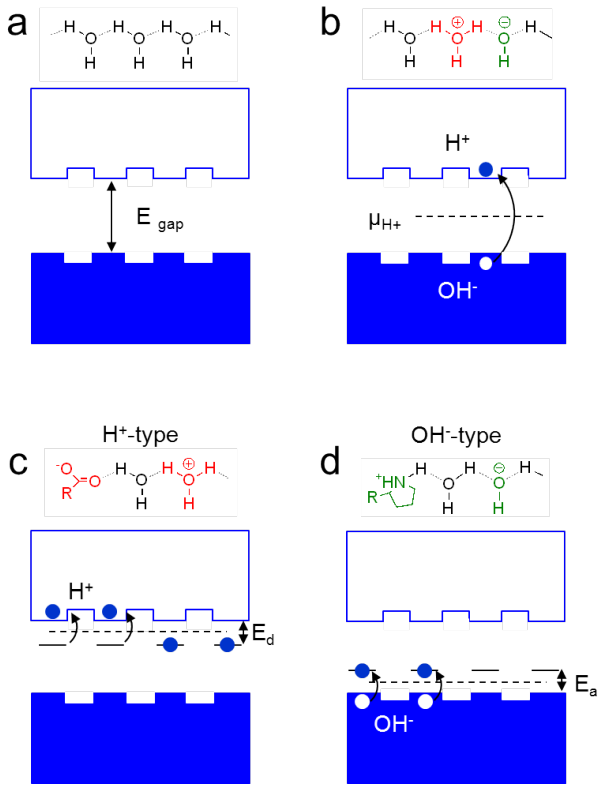

Figure 4.1. Protonic semiconductor model. a) Quasi-band proton wire description, b) formation of a H^+ and OH^- pair requires 0.83 eV activation energy and makes the wire conductive, c) acid groups in the polymer donate H^+ and create a H^+-type proton wire, d) base groups in the polymer accept H^+ and create a OH^--type proton wire.

The conductivity of proton wire can be changed by doping with H^+ or OH^- like doping in semiconductors. The number of acid or base groups in the protonic conducting materials will affect the concentration of free protons, thus the charge carrier density will influence the conductivity. The dissociation constant of an acid/base will define its activation energy. Using the same Gibbs-Helmholtz equation, $E_{gap}=-k_BTlnK_w$, but substituting water dissociation constant K_w to acid/base dissociation constant K_a/K_b to calculate the activation energy. For an acid H^+ donor, acidic group can donate a H^+ to the proton wire "conduction band", as a dopant from Group V (Phosphorus) to Si (Figure 4.1 c). Since $pK_a=-logK_a$, the activation energy can be calculated as E_{donor} using the pK_a value of the acid. The pK_a of maleic chitosan is about 3.2.[50] According to the above equations, we estimate the activation energy for maleic chitosan is about 0.19 eV. We then put the proton donor groups at E_{donor} = 0.19 eV below the proton conduction quasi-band. A basic functionality of proton wire can accept a H^+ to form a OH^- in the "valence band", like a dopant from Group III (Boron) creating a hole in the valence band of Si (Figure 4.1 d). Knowing pK_b of the base, energy for the acceptor can be calculated. For a base H^+ acceptor, we have its activation energy as E_{acc}. In analogy to acid doped maleic chitosan (H^+ donating), unmodified chitin is the intrinsic form of a H^+ conductor. Chitin can form H-bonded water network but does not have an acid or base functional group. Bulk film test was done with a chitin film (Figure 4.2 a). Pd contacts were used and the humidity level was kept at 75% RH with H_2 flow. 5 mL 0.5% (w/v) chitin HFIP solution was dropped on a clean Teflon plate.[80] After drying for about one hour, a thin layer of film formed and was peeled off and sandwiched between two Pd contacts. Chitin film showed very low conductivity compared to maleic chitosan. Chitin can also form hydrogen bonding network. But because there are no proton donor groups in chitin structure, the charge carrier density is low. As expected, the H^+ conductivity of chitin is significantly smaller than maleic chitosan (Figure 4.2 b). H^+ conduction has been proved in both intrinsic and H^+-type protonic conductors. In the following sections, I am going to describe a base doped (OH^--type) H^+ conductor and provide a preliminary demonstration of its protonic conductivity.

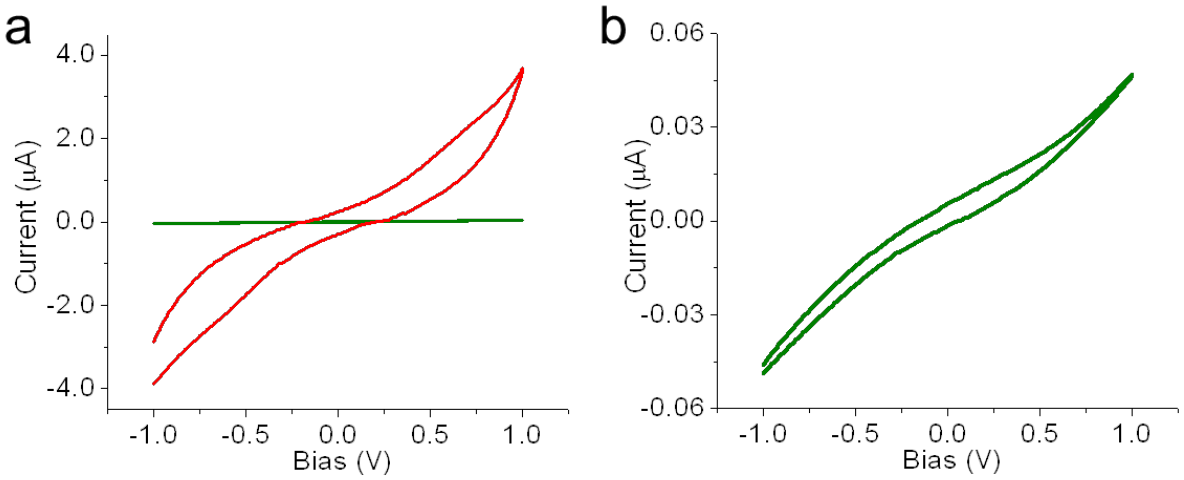

Figure 4.2. Proton conductivity of chitin and maleic chitosan. (a) Chitin (green) and maleic chitosan (red) measured at 75% RH with PdH contacts in 5% H_2. (b) is the enlarge of chitin current from (a). Contact area is 1 cm^2; film thickness is ~300 μm each.

4.3 OH^--TYPE MATERIAL SYNTHESIS

Here, I demonstrate the synthesis of a positively charged chitosan derivative, proline chitosan, which contains an ionizable base group on the side chain. I followed previously reported quaternization reaction mechanism that was able to overcome the solubility issues encountered during the functionalization of chitosan.[81] More specifically, the primary amine groups on the chitosan side chain are first protonated and form a quaternary ammonium compound, which then allows for the modification of chitosan with either acidic or basic chemical functionality. This type of modification is desirable because it retains the functionality of the chitosan backbone and enhances the water-solubility of the product. Proline is chosen as the functional group in the OH^--type material. Proline is a weak base, of which the conjugated acid has a pK_a value of about 3.2. The pK_a is comparable to the acidity of maleic acid group in the H^+-type proton conductor.

Proline chitosan synthesis (Figure 4.3) was done with our collaborator Dr. Brett A. Helms at the Molecular Foundary of Lawrence Berkeley National Lab. Chitosan powder (1 g) was dissolved in formamide (200 mL) with the assistance of methanesulfonic acid (0.4 mL). Upon the addition of the acid, the primary amine in chitosan (pK_a = 6.5) becomes protonated and assists the solubility in the organic solvent. After stirring for 12 h at ambient temperature, the solution becomes transparent and viscous. Subsequently, proline solid (4.1 g, 4-fold in molar ratio of sugar units) and 6.8 g 1-ethyl-3-(3-dimethylaminopropyl) carbodiimide (EDC) are then dissolved in deionized water. The proline mixture is slowly added into the chitosan solution, and the pH is adjusted with 0.1 M $NaHCO_3$. The reaction takes place while stirring at 60 °C for 24 hrs. The product was dialyzed in deionized water (MW cut off 12,000 Da) for 5 days, with fresh deionized water changed every day, to eliminate the free acetic acid, $NaHCO_3$ and isourea. The solution was finally lyophilized (Thermo Fisher Scientific) for 3 days to obtain proline chitosan.

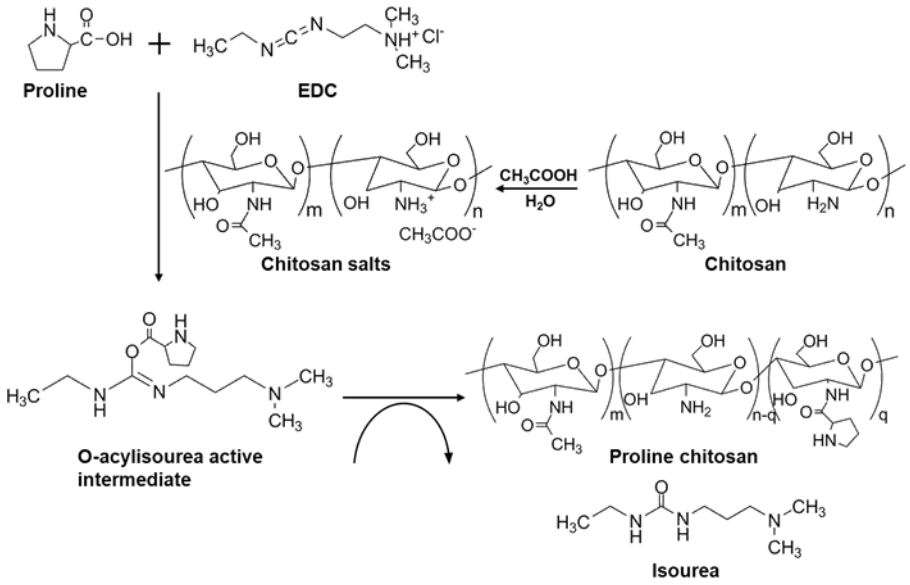

Figure 4.3. Molecular structure and synthesis process of proline chitosan.

FTIR analysis was performed to ascertain the success of the synthesis reaction. The IR spectrum of proline chitosan was compared with chitosan. Both chitosan and proline chitosan powder were mixed with KBr (sample/KBr 1:100 w/w), and then compressed into pellets. FTIR spectra were obtained with a Bruker Vector 33 FTIR spectrophotometer. As shown in Figure 4.4, the peaks representing chitosan at 3450 cm^{-1} (O-H stretching), 1655 cm^{-1} and 1630 cm^{-1} (amide I), 1160 cm^{-1} (bridge oxygen stretching), 1070 cm^{-1} and 1030 cm^{-1} (C-O stretching) are present in both samples. [82] But the peak intensity of amide I is much stronger than C-O stretching in proline chitosan compared with chitosan, which is indicative of the amide bond formation resulting from the reaction between carboxyl groups of proline and primary amines of chitosan. H NMR analysis was also done with proline chitosan. But the signal from amide bond is too small to compare with the proton signals from the chitosan backbone.

The degree of substitution (DS) can also be determined from FTIR using the peak area ratios of $A_{1655,\text{-NH-}}/A_{1070,\text{C-O}}$, following previous literature procedures.[80] The absorption intensities of amide I (1655 cm^{-1}) and C-O stretching (1070 cm^{-1}) were measured respectively on the baseline from 1800 cm^{-1} to 1600 cm^{-1} and the baseline from 1220 cm^{-1} and 860 cm^{-1}. $A_{1655,\text{-NH-}}/A_{1070,\text{C-O}}$ values of 0.34 for chitosan and 0.75 for proline chitosan were obtained based on the calculation. For chitosan with $A_{1655,\text{-NH-}}/A_{1070,\text{C-O}} = 0.34$, the degree of deacetylation is 0.75.**[82]** The amount of acetyl groups (the same as amide bond) in chitosan sample is 1-0.75=0.25. In chitosan, as shown in Figure 4.4, the $A_{1655,\text{-NH-}}/A_{1070,\text{C-O}}$ ratio between amide and C-O bond is m/(number of C-O). We found $A_{1655,\text{-NH-}}/A_{1070,\text{C-O}}$ to be 0.34 and m=0.25. In proline chitosan, the $A_{1655,\text{-NH-}}/A_{1070,\text{C-O}}$ ratio increased to 0.75. In both samples the number of C-O bonds didn't change. The increased $A_{1655,\text{-NH-}}/A_{1070,\text{C-O}}$ ratio value resulted from the amide bonds formation due to proline attachment. Here, $A_{1655,\text{-NH-}}/A_{1070,\text{C-O}}$ equals to (m+q)/(number of C-O)=0.75. We found m=0.25 from chitosan, so q=0.31. The degree of substitution of proline chitosan is 0.31.

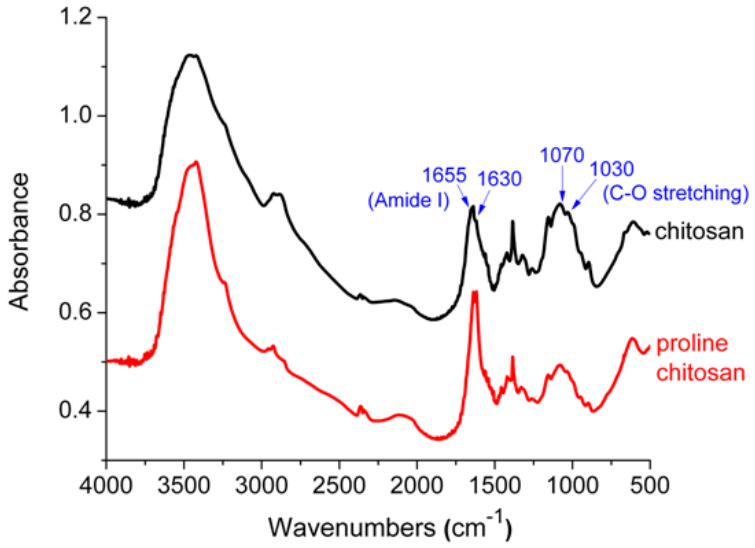

Figure 4.4. FTIR spectra of chitosan (black) and proline chitosan (red)

4.4 OH^--TYPE PROTON CONDUCTOR

The conductivity of proline chitosan was first measured with a PdH_x sandwiched device. 1 cm^2 PdH_x contacts and 2 mL of 3.5 wt% proline chitosan aqueous solution were used. The same method to make maleic chitosan sandwiched device was described in Chapter 2.3. Two-terminal device was measured in 75% RH and a 5% H_2 atmosphere. As a control, separate measurements were conducted either with gold (Au) contacts or with Pd for proline chitosan film. Both Au and Pd are poor proton conductors and better electronic conductors compared to PdH_x. The current for PdH_x is higher than Pd or Au contacts (Figure 4.5 a).

In order to verify the formation of the hydrogen bonded network in proline chitosan, the electrical dependence of proline chitosan on the humidity is showed in Figure 4.5 b. Measurement was done with a two-terminal PdH_x sandwiched proline chitosan thin film device and tested in 5% H_2 atmosphere. As expected, a higher humidity results in a more thoroughly hydrated device and an increased current. Measurements were conducted up to 75% humidity; above this level water condensation results in dramatic hysteresis and noise.

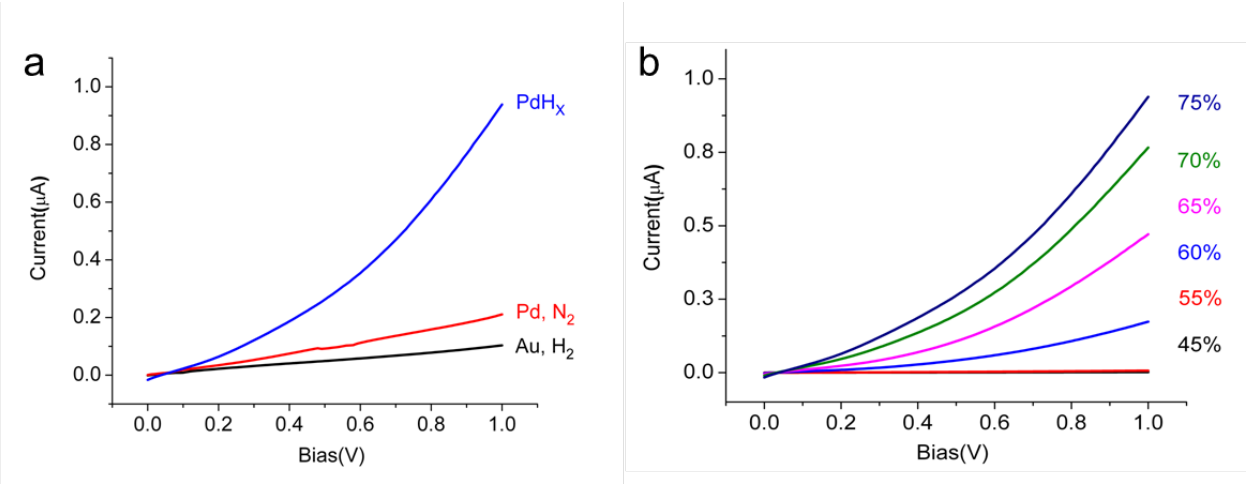

Figure 4.5. Proton conductivity of OH^--type proton conductor. (a). Proline chitosan measured with: PdH_x contacts in 5% H_2 (blue), Au contacts in 5% H_2 (black), Pd contacts in N_2 (red). The humidity is constant at 75%, (b). Conductivity as a function of humidity for proline chitosan measured with PdH_x contacts.

4.5 H^+-TYPE OH^--TYPE JUNCTION DEVICE

As part of their model that compares H^+-type and OH^--type protonic semiconductors with electronic semiconductors, Eigen and de Mayer propose a H^+ - OH^- junction in ice with acid and base dopants.[10] Similarly, here we measure the properties of maleic-chitosan (H^+-type) and proline-chitosan (OH^--type) junction devices with proton conducting contacts under 75% RH (Figure 4.6). When a potential difference between the contacts is applied (V_{MP}), the measured current (I_{MP}) shows asymmetric characteristics as expected (Figure 4.6 a). The dependence of I_{MP} on V_{MP} in the H^+ -OH^- junction is easily described with the semiconductor model (Figure 4.6 b, c). At first contact, the gradient in μ^{H+} drives the diffusion of H^+ into the proline-chitosan and OH^- into the maleic-chitosan until equilibrium is reached. The charge carriers recombine at the junction as H_2O and create a depletion region with an associated contact potential (V_0) (Figure 4.6 a). This H_2O generated at the interface does not affect the hydration of the polymers at the interface because the overall concentration of the recombined H^+ and OH^- is negligible compared to the water already existing in the biopolymers. A positive potential on the H^+-type side (forward bias) reduces V_0 and results in a net thermally activated current of H^+ and OH^- across the forward biased junction (Figure 4.6 c). At the same time, a negative potential on the H^+-type side increases the potential barrier and results in very little or no current going across the reverse biased junction. This model is used to simulate the junction characteristics (Figure 4.6 a). We treat the maleic-chitosan and the proline-chitosan as n-type and p-type electronic semiconductors (switching the sign of the charge carriers) following the semiconductor model (Figure 4.1 c, d) with a band gap of 0.8 eV. The number of H^+ donated by the maleic-groups (Figure 2.3a) in the proton "conduction band" is derived from the H^+-FETs (Chapter 4.7). In turn, the number of OH^- proton holes created by the proline-base in the proton "valence band" (Figure 4.3) is calculated from the OH^- FETs (Chapter **Error! Reference source not found.**). The contribution to the charge carrier doping of the unreacted - NH_2 in chitosan can be neglected. The dissociation constant of these amines (pK_b= 7.5) is low compared to the dissociation of the proline or the maleic groups. The mobility data for the charge carriers is also derived from the H^+-FET and OH^--FET devices (Chapter **Error! Reference source not found.**). In the forward bias region, the overall shape of the curve matches the shape of the experimental data well for a minority carrier recombination time of 1 μs. This recombination time is remarkably close to the recombination

time of H^+/ OH^- in neutral water (35 μs)[10] and appropriately smaller because of higher H^+/OH^- concentration in the devices. Despite the applied voltages being below electrolysis levels, the increased back bias current may be due to field-induced water splitting at the contacts as previously observed in bipolar ion-exchange membranes.[83] To appropriately simulate the experimental conditions, we scale the current in a 1x1 μm^2 junction by several fold, but not by the exact amount required to recreate exactly a junction with 1x1 cm^2 contacts. The H^+-type OH^--type junction is assembled from pre-formed components and results in a device with overall poor physical contact. This poor physical contact effectively reduces the area of the junction and the area of the contacts. Despite these shortcomings, the junction devices show the expected rectifying behavior, which is qualitatively matched by the simulations.

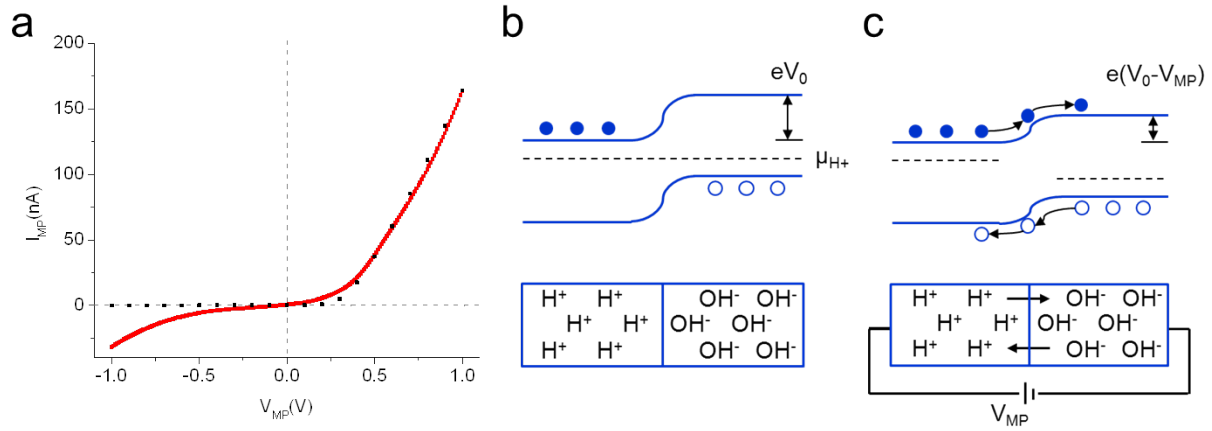

Figure 4.6. H^+-type and OH^--type junction device. (a) Red trace: experimental data for IV characteristics of a H^+/OH^- junction formed by maleic chitosan and proline chitosan. The curve shows the expected nonlinearity. Black dots: data from simulations for the same junction using the semiconductor model. (b) When a H^+ doped and OH^- doped material are placed into contact OH^- diffuse into the H^+ region and H^+ diffuse into the OH^- region until the μ_{H+} on both sides is the same. H^+ and OH^- recombine in the depletion region. A contact potential V_0 occurs across the junction and is dependent of the difference in μ_{H+} of both sides. (c) A forward bias (+ive on H^+ side) applied between source and drain reduces the contact barrier $e(V_0-V_{MP})$ and thermionic emission of H^+ into OH^- side and vice versa occurs.

4.6 COMPLEMENTARY FIELD EFFECT TRANSISTORS

In a H^+-FET type device (Figure 3.1), the source-drain protonic current, I_{DS}, recorded as a function of drain-source bias, $V_{DS,}$ is controlled by changing the potential of the back gate electrode, V_{GS}. As previously reported,[50] for the maleic-chitosan H^+-FET (Figure 4.7 a), a negative V_{GS} results in a higher source-drain current for the same V_{DS}, while a positive V_{GS} almost turns I_{DS} off. This V_{GS} dependence of I_{DS} is consistent with an FET with positive charge carriers (H^+). In turn, the proline-chitosan OH^--FET shows the opposite V_{GS} dependence. A negative V_{GS} almost turns the device off and a positive V_{GS} results in higher I_{ds} (Figure 4.7 b). This V_{GS} dependence of I_{DS} is consistent with an FET with negative charge carriers (OH^-).

We explain the I_{ds} modulation from V_{GS} in these devices with the gradual channel approximation:[84]

$$I_{DS} = \pm \mu_{lin} C_G \frac{W}{L}[(V_{GS} - V_{TH})V_{DS}] \quad (1.2)$$

(+ for a negative charge carrier and – for a positive charge carrier, μ_{lin}=mobility in the linear regime, C_G= gate capacitance per unit area, W=device width, L= device length, V_{TH}=threshold gate voltage at which conduction occurs).

A few modifications are required to equation (1.2) to take into account that in our accumulation mode devices we cannot reach the V_{TH} at which the channel is completely depleted of charge carriers. We first rewrite equation (1.2):

$$J_{DS} = \pm \mu_{lin} \frac{C_G}{t} V_{GS} \varepsilon_{DS} \quad (1.3)$$

(J_{ds}= source drain current density, $C_{GS}V_{gs}/t$= charge carrier per unit volume induced by the gate, $\varepsilon_{DS}= V_{DS}/L$=electric field along the device channel) and compare it to

$$J_{DS} = \sigma \varepsilon_{DS} = e \mu_{lin} n \varepsilon_{DS} \quad (1.4)$$

(σ= channel conductivity, n=charge carriers per unit volume, e=elementary charge). We then modify n to take into account for the H^+ (n_0^{H+}) or OH^- (n_0^{OH-}) from acid and base doping already in the channel at V_{GS}=0. This modification results in

$$n^{H+} = n_0^{H+} - \frac{C_G V_{GS}}{et} \quad (1.5) \text{ for } H^+\text{-FET}$$

and $n^{OH-} = n_0^{OH-} + \frac{C_G V_{GS}}{et}$ (1.6) for OH^--FET respectively (Figure 4.7 c, d).

Using equation (1.5) and equation (1.6), equation (1.3) becomes

$$J_{DS} = e\mu_{lin}^{H+}(n_0^{H+} - \frac{C_G V_{GS}}{et})\varepsilon_{DS} \quad (1.7)$$ for H^+-FET, and

$$J_{DS} = e\mu_{lin}^{OH-}(n_0^{OH-} + \frac{C_G V_{GS}}{et})\varepsilon_{DS} \quad (1.8)$$ for OH^--FET.

To calculate μ_{lin}^{H+}, μ_{lin}^{OH-}, n_0^{H+} and n_0^{OH-}, we plot $\frac{\partial J_{DS}}{\partial \varepsilon_{DS}} = \sigma$ as a function of V_{GS} (Figure 4.7 e, f).

μ_{lin}^{H+}, μ_{lin}^{OH-}, are derived from the gradient of the linear fit and n_0^{H+} and n_0^{OH-} are derived from the intercept (Figure 4.7 e, f).[84] From the devices, $\mu_{lin}^{H+} = (5.3 \pm 0.5)10^{-3}\,cm^2V^{-1}s^{-1}$ and $\mu_{lin}^{OH-} = (0.40 \pm 0.02)10^{-3}\,cm^2V^{-1}s^{-1}$. The mobility for H^+ is remarkably close to the mobility for H^+ in diluted acidic solutions.[85] For basic solutions, the mobility of OH^- is lower than H^+ and reported as 1.96 x 10^{-3} cm^2 V^{-1} s^{-1}. Our OH^--type devices show a mobility that is reasonable agreement, but is five-fold lower than expected. A few factors may contribute to the lower than expected OH^- mobility. The proline chitosan in the OH^--FET contains less water (15% *w/w*) than the maleic-chitosan in the H^+-FET (20% *w/w*). This lower water content results in a smaller number of pathways, or proton wires, for the OH^- to conduct. In the analysis, we have neglected the effects of contacts. It is conceivable that the contact between the PdH_x and the proton-conducting channels is affected by the difference in protochemical potentials. From the data for the PdH_x reversible electrodes in acidic solutions,[43] one infers qualitatively that the protochemical potential of the PdH_x is closer to the protochemical potential of the H^+-type maleic chitosan and is significantly higher than the protochemical potential of the OH^--type the proline chitosan. PdH_x is thus more likely to form a better protonic contact (Ohmic) with maleic-chitosan, while a potential barrier at the PdH_x- proline-chitosan contact may occur. This barrier is similar to a Schottky barrier that occurs between a metal with low work function and a p-type electronic semiconductor. This potential explanation, however, requires further investigation and will be addressed in future work. With the values of the mobility, we extrapolate $n_0^{H+} = (8.0 \pm 0.4)10^{17}\,cm^{-3}$ and $n_0^{OH-} = (4.0 \pm 0.1)10^{17}\,cm^{-3}$ for the devices. The values are compared with $n_{maleic}^{H+} = 8.9 \times 10^{17}\ cm^{-3}$ $n_{proline}^{H+} = 4.3 \times 10^{17}\ cm^{-3}$ derived from the acid and base

doping semiconductor model (Chapter 4.2). Given all the assumptions made in deriving the values from the acid and base doping, the agreement is good. This agreement confirms that the semiconductor model is an appropriate description for proton transport in proton wires measured with our devices.

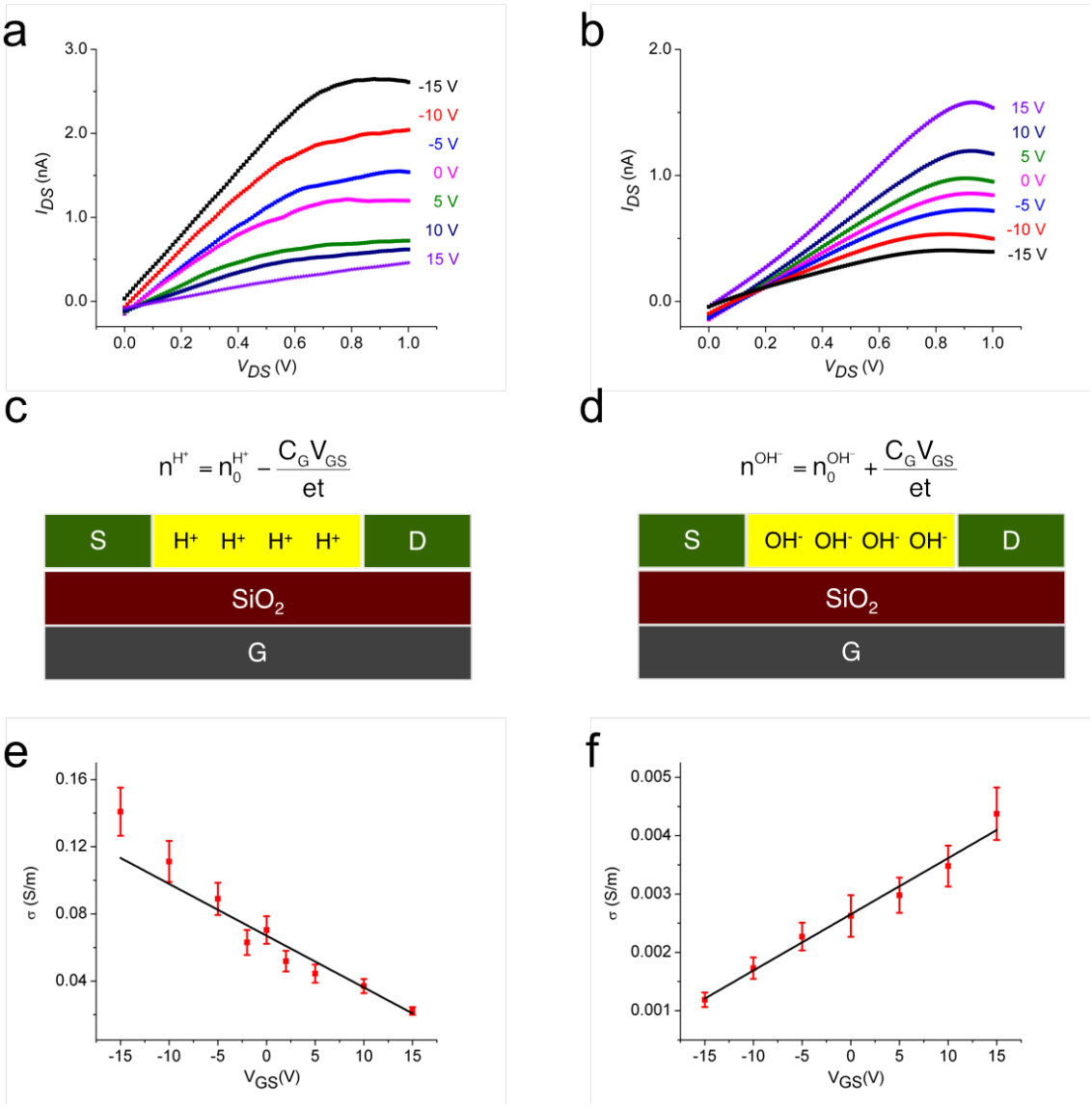

Figure 4.7. OH^--FET. (a) (b) Plots of I_{DS} as a function of V_{GS} for different V_{DS} (RH 75%) for a maleic chitosan H^+-FET and a proline chitosan OH^-FET with PdH_x contacts. Device dimensions: length 8.6 μm, width 3.5 μm, height 82 nm for (a) and 9.6 μm, width 28 μm, height 200 nm for (b). (c) (d) Schematics of H^+ and OH^- transistor capacitative charge carrier n^{H+} and n^{OH-} modulation. From simulations of dQ/dV_{gs}, $C_g = 3.85 \times 10^{-4}$ F m^{-2}. (e)(f) Plots of $\frac{\partial J_{DS}}{\partial \varepsilon_{DS}} = \sigma$ as function of V_{GS} and linear fit for the device in (a) and (b) respectively. For cross σ and charge density calculations the cross sectional area of the devices was derived from AFM and the cross sections were approximated to a rectangle with t= 66 nm for (a) and t= 160 nm (b) with the same widths as the actual devices.

4.7 CONCLUSION

In summary, I studied H^+-OH^- rectifying junctions and H^+-type and OH^--type complementary field effect transistors with polysaccharide based biomimetic proton wires. These devices confirm that proton wires support the conductivity of OH^- as proton holes. The conductivity in these devices was described with a model in which H^+ (protons) and OH^- (proton holes) are equivalent to electrons and holes in semiconductors. Originally Eigen and de Maeyer proposed this model. Together with Prof. Rolandi, we refined the model to include band gap calculations and effects of doping on the protochemical potential. The mobility for H^+ and OH^- in our devices, $\mu_{lin}^{H+} = (5.3 \pm 0.5)10^{-3}\,cm^2V^{-1}s^{-1}$ and $\mu_{lin}^{OH-} = (0.40 \pm 0.02)10^{-3}\,cm^2V^{-1}s^{-1}$, are in good and reasonable agreement with what has been previously reported for the same species in other hydrogen-bonded systems. These H^+-FETs and OH^--FETs with biocompatible polysaccharides represent a versatile platform for bioelectronics (bioprotonics) to measure and control physiological functions affected by H^+ and pH. The ability to precisely control the flow and concentration of H^+ and OH^- may also be used to study the kinetics of acid-base chemical reactions.[86]

Chapter 5. PH MODULATOR

Abstract

An electrochemical setup is used to investigate the H^+ transfer between the protodes and solution. Voltage applied between the working electrode and the reference electrode controls the H^+ transfer. Substituting the conventional platinum (Pt) counter electrode to a high capacitance electrode used in electric double layer capacitor (EDLC) can store the H^+ concentration change in the solution, thus changing the pH. The pH sensitive firefly bioluminescent reactions are integrated as the device readout.

5.1 INTRODUCTION

H^+ concentration in solution is pH value. pH is one of the most potent intrinsic neuromodulators within the brain.[3, 87] H^+ ion exerts powerful actions on neuronal function based on the high H^+ sensitive protein molecules, including voltage-gated channels, ion pumps and enzymes.[88] Some research has suggested that proton may function as a neurotransmitter, which can regulate synaptic plasticity in the brain.[3] Localized acidosis reduces neuronal excitability and has been proposed to stop epileptic seizures.[89, 90] Conventional methods to change fluid pH are to flow CO_2 gas or titrate with H_2CO_3 solution.[91] Both methods change the whole cell medium pH, lacking the ability of local control. Microelectrodes can be integrated with neurons and stimulate neural functions by applying electrical signals. Although pH sensitive microelectrodes already exist,[92] microelectrodes that can control H^+ concentration locally are still lacking. Thus, modulating neuron cell behavior with H^+ selective electrodes will bring a new perspective to neuronal disease diagnosis and therapy.

Cells remain the functions normally within a small range of pH change. The pH value outside mitochondria fluctuates between 7.4-7.6.[93] Cell medium regulates or maintains the pH to be stable, acting like a buffer. So drastic ion concentration changes from outside will not easily interrupt cell functions. Such ability of a buffer solution is described as buffer capacity or buffering power. Physiologically relevant pH ranges from 6.5 to 8.0.[88] The buffering power (β) of an aqueous solution is defined as the change in pH arising per incremental concentration change of strong base or acid.

$$\beta = \frac{db}{dpH}, or\ \beta = -\frac{da}{dpH}$$

where *db* and *da* represent incremental changes in the concentration of strong base or strong acid, respectively. The unit of buffering power is in terms of concentration. The total intracellular buffering capacity of neurons and glial cells is on the order of 30-50 mM.[88]

Neural cell medium has a pH value of 7.3 and buffer capacity of 50 mM. When using acidosis as epileptic seizure treatment, normally 1 unit of pH change is required. So 0.05 mol/L (50 mol/m^3) H^+ concentration change is needed to reach pH 6.3. While for regular solution, 10^-6 mol/L H^+ concentration is able to achieve the pH change. Or the 0.05 mol/L H^+ can change the pH from 7.3 to 2 for a non-buffer environment.

Chapter 5.2 is presented in a similar form as it was published in Applied Physics Letters Materials (Miyake T. … Deng Y. et al., An enzyme logic bioprotonic transducer, Applied Physics Letters Materials, 3, 014906 2015, http://dx.doi.org/10.1063/1.4900886). Reproduced with permission from APL Materials.

5.2 H^+ Transfer Between Protodes and Solution

The protonic devices use PdH_x protodes to inject H^+ into the proton conducting polymer channel. Formation of PdH_x requires hydrogen gas as proton source. However, the common media for biological systems is solution. In order to integrate with biological systems, the protonic devices need the conversion of a H^+ current from solution. To this end, I exploit the electrochemical properties of the PdH_x formation and its dependence on the voltage applied on the contact (Figure 5.1).[94] To calibrate the protonic transducer, together with Dr. Takeo Miyake we first investigate the dependence of the formation and depletion of PdH_x on the potential applied to the metal. For this measurement, we prepare Pd films (100 nm thickness) on glass slides by electron beam deposition, and measure the electrochemical current at the Pd electrode (0.2 cm^2 surface area) in a 0.5 M Na_2SO_4 solution (pH 6.7). We use the standard three-electrode system with Ag/AgCl as the reference electrode (RE) and platinum (Pt) as the counter electrode (CE, 0.5 cm^2 surface area) (Figure 5.1 a). First, we form PdH_x with a negative V applied to the PdH_x working electrode (WE), which we refer to as a cathodic voltage V_c. A V_c applied to the Pd induces a reduction current of e^- to flow into the Pd, which we refer to as cathodic current (I_c). These e^-

reduce the H^+ from solution, which are adsorbed as H into the Pd to form PdH_x. Second, once the Pd is fully converted to PdH_x with x = 0.6, we switch V to a positive anodic voltage (V_a) at which PdH_x is expected to return to Pd. For this specific measurement, V_a = 0 V. The difference in chemical potential of H^+, or protochemical potential (μ) between the PdH_x (μPdH) and the solution (μpH), determines whether the H^+ will transfer back to the solution. This difference is defined as[38]

$$\mu_{pH} - \mu_{PdH} = eV + k_B T \ln\left(\frac{a_{H+}}{(pH_2)^{1/2}}\right) \quad (1.9)$$

where a_{H+} = activity of H^+ in solution with pH = -log a_{H+}, pH_2 = hydrogen partial pressure in the Pd.

From the equation (1.9), the protochemical potential of H^+ in the PdH_x (μPdH) for x = 0.6 and V = 0 V is the same as the protochemical potential for a solution at pH = 0 (μpH=0), and higher than the protochemical potential for a solution at pH = 6.7 (μpH=6.7).[95] While hydrogen transport through the PdH_x electrode causes overpotential in protochemical potential, this overpotential is negligibly small.[48]

As a result, for V_a = 0 V, H^+ flow from PdH_x into the solution and induce an oxidation current of e^- to flow from the electrode. This current is a product of the oxidation of H from the PdH_x into H^+ (Figure 5.1 b) and we refer to it as anodic current (I_a). Since I_c is affected by dielectric charging of the solution, we use the magnitude of I_a to measure the extent of PdH_x formation for a given V_c assuming that for a specific V_a all of the H^+ loaded onto the Pd for V_c returns to the solution. During the formation of PdH_x, we also observe a color change in the electrode from metallic (Pd) to white (PdH_x), while after depletion the electrode returns to its original metallic color (Pd).[96] The formation of PdH_x does not occur for every value of V_c. At pH 6.7, I_a at V_a = 0 V drops by an order of magnitude between V_c = -1.0 V and V_c = -0.9 V indicating that formation of PdH_x did not occur for V_c > -1.0 V. We assume that the threshold voltage for formation (at pH 6.7) is V_c = -1.0 V. Similar to formation, the depletion of PdH_x is also governed by differences between μPdH and μpH and exhibits a threshold behavior. For fully loaded PdH_x, I_a is close to 0 for V_a < -0.3 V (in a pH 6.7 solution). During depletion of the contact, we calculate the total charge transferred from the PdH_x to the solution by integrating I_a as function of time.[96]

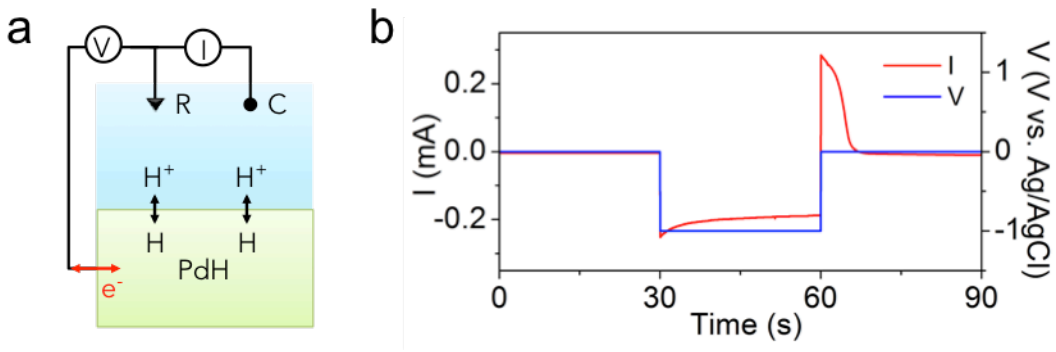

Figure 5.1. H^+ transfer between PdH_x and solution. (a) Voltage-controlled Pd/ PdH_x behavior. Electrons and protons travel into the Pd/ PdH_x during formation and out of it during depletion. (b) Temporal characteristics of the PdH_x formation (V_c = -1.0 V) and depletion (V_a = 0 V) in pH 6.7 Na_2SO_4 solution.

Second, we investigate the dependence of the PdH_x formation and depletion on the solution pH (Figure 5.2). We determine the threshold values for V_c and V_a for a range of pH values (0.0, 2.0, 3.0, 4.5, 6.7, and 11.0) (Figure 5.2a). As solution pH increases, the threshold values for V_c and V_a decrease, as expected due to the influence of pH on the solution protochemical potential.[95, 97] It is interesting to note that there is a range of pH and V (area in white) in which the solution and the PdH_x are in equilibrium and no exchange of H^+ across the interface occurs. To further elucidate the depletion dynamics, we measure I_a as a function of solution pH by pre-loading the Pd with H_2 gas rather than loading electrochemically from solution. When exposed to H_2 gas, Pd absorbs H_2 to form PdH_x with $x = 0.6$ for $0.1 \text{ atm} < H_2$ pressure < 1 atm.[9, 45] As expected, at $V_a = 0$ V, I_a for a solution with a low proton concentration (e.g., pH 11) is larger than I_a from a solution with a high proton concentration (e.g., pH 2), and no depletion occurs at pH 0 because $\mu pH = 0 = \mu PdH$. This is because an increase in proton concentration at the protode surface results in a smaller protochemical potential difference between the loaded PdH_x contact and the solution. The opposite is true for the formation of PdH_x. As the proton concentration at the protode surface is increased (lower pH), the favorability for the reduction is also increased. Importantly, we find that the threshold potentials for formation (V_c) and depletion (V_a) vary as the solution pH varies. When the reaction is proceeding very slowly, the calculated formation threshold voltage depends on the reaction rate in addition to activation energy, which probably causes the non-linear results for threshold V_c (Figure 5.2 b).

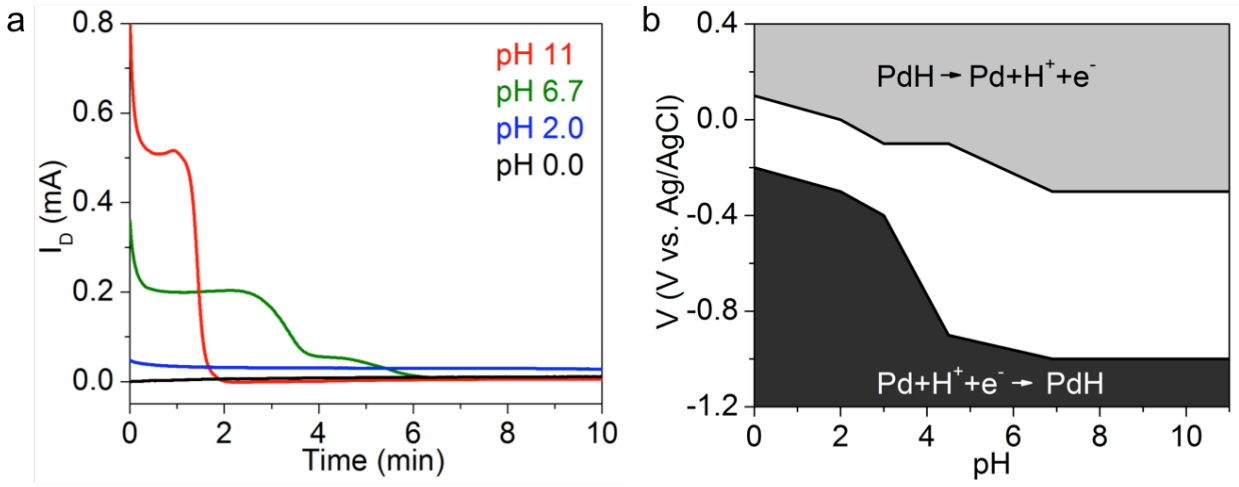

Figure 5.2. pH and voltage dependence of PdH_x formation and depletion in solution. (a) Current from PdH_x protodes held at V_a = 0 V during depletion. At high pH, depletion occurs rapidly and at low pH, depletion occurs slowly. Depletion was measured by first absorbing H_2 in gas phase for 40 min (pH_2 in air = 0.2 atm), then immediately reducing the voltage to the value of interest and checking for positive depletion current. (b) Dependence of formation and depletion on pH and voltage. Formation was measured by absorbing protons for 60 s at given pH and applied V_c, then testing for a significant I_a. If the depletion current increased by more than an order of magnitude, formation occurred.

5.3 pH MODULATION IN SOLUTION

The applied voltage can control H^+ flow in and out of the PdH_x contacts. The concentration of H^+ in solution reflects as the pH values. Figure 5.2 b shows the effect of solution pH on PdH_x formation and depletion. If the device could reserve the H^+ in solution, V_c and V_a can modulate the solution pH.

In order to achieve this function, the common Pt CE used in Figure 5.1 a setup would not work because of the high catalytic property of Pt. Redox reactions ($4H^+ + O_2 + 4e^- \rightarrow 2H_2O$, $2H^+ + 2e^- \rightarrow H_2$, $2H_2O + 4e^- \rightarrow H_2 + 2OH^-$) on the CE would balance the H^+ injected from the WE. The alternative is to use the electrodes that are inert but also with high capacitance, similar as the electrodes used in electrochemical double layer capacitors (EDLCs).[98] Those electrodes eliminate Faradic reactions and have high capacitance per unit area due to high specific surface area. Thus ions adsorb on the electrode surfaces to store energy for the electrochemical capacitor. Dr. Miyake has developed a carbon nanotube modified carbon fiber electrodes (CF/CNT) to be used in EDLCs. The capacitance of CF/CNT is C_i = 6.5 mF/cm^2.[99] With the CF/CNT, when applied V_c to Pd, H^+ are transferred from solution into the WE to form PdH_x. At the same time, anions in the solution adsorb on CF/CNT. Due to the H^+ concentration decrease in the solution, there is a pH increase in the solution (Figure 5.3 a). When V_a (big enough for PdH_x depletion) is applied, PdH_x injects H^+ into the solution. CF/CNT releases the anions to keep charge balanced in the solution. The pH of the solution returns to its original (Figure 5.3 b). With the inert CF/CNT, it is possible to observe a pH change in solution. Although, the CF/CNT can't eliminate all the redox reactions on the counter electrode, yet it would store the ions for the pH control.

I_a is recorded during the process to track PdH_x formation (Figure 5.3 c). Without loading (I_c) process I_a is much lower (dashed green line in Figure 5.3 c). V_c = -0.9 V and V_a = 0.9 V are determined from the process map in Figure 5.2 b. During the process, I add a universal pH indicator into the solution to monitor the pH change. To rule out the influence of dissolved oxygen in solution, I perform the test with degassed Na_2SO_4 solution. Pure nitrogen gas is bubbled into 5 mL pH 6.5 Na_2SO_4 solution for at least 1 hour prior to use. 1 mL of the degassed solution is added into the test chamber. During the test, nitrogen gas is gently flown on top of the solution to prevent any gas dissolution. V_c = -0.9 V at the WE transfers H^+ from solution into the

contact. H^+ combines with e^- and forms H. H adsorbs on Pd surface to form PdH_x. Loss of H^+ induces pH increase in solution. pH indicator changes from light green (neutral pH) to purple (basic pH) (Figure 5.3 d,e). Pd WE also changes from metallic silver color into tarnished PdH_x color. When reversing the voltage to $V_a = 0.9V$, pH indicator returns to its original color (Figure 5.3 f). pH indicator shows a more obvious color change at the electrode surface; existence of Debye layer where the ions accumulate. Same test with gold WE doesn't show same color change as Pd WE. Gold can't adsorb H as Pd does. H^+ remain in solution instead of being transferred into the contact.

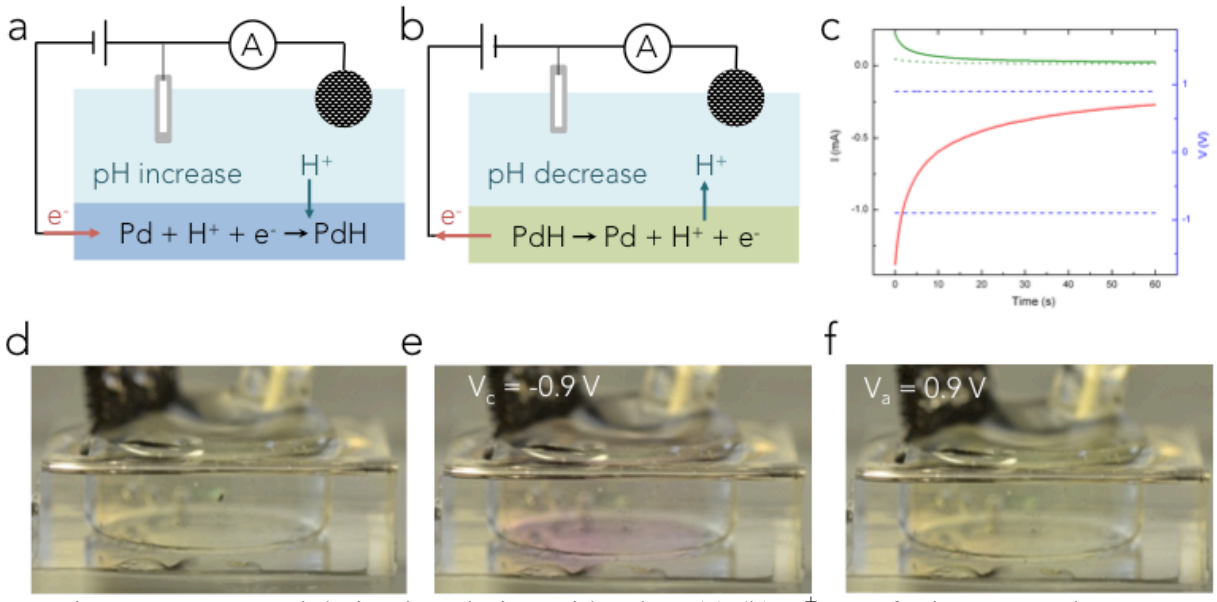

Figure 5.3. pH modulation in solution with PdH_x. (a) (b) H^+ transfer between PdH_x WE and solution induces pH change in solution; (c) Characteristics of I_a and I_c in pH 6.5 Na_2SO_4 solution; (d) pH indicator green shows pH neutral in solution; (e) pH indicator purple indicates basic pH. (f) pH indicator returns to original color.

5.4 BIOLUMINESCENCE

In nature, living organisms can emit light, known as bioluminescence. The familiar yellow-green glow of the firefly is a beautiful example of bioluminescence. The light emitting reaction is based on the oxidation reaction of firefly luciferin, catalyzed by the luciferase enzyme. Luciferin is oxidized into oxy-luciferin, utilizing ATP as the energy source and consuming Mg^{2+}. The light emitting reaction of firefly luciferin is pH sensitive.[100] DeCoursey et. al. has reported the finding of proton sensitive ion channels in jellyfish.[101] Dr. Takeo Miyake purchased a Japanese toy, Photalight, which contains one package of firefly luciferin and ATP powder, and the other package of luciferase. We mix the two packages of powder together in different pH buffer solutions and observe different color of light (Figure 5.4 a). The optimal pH of the enzyme reaction is at pH 8, showing green color. A more basic pH induces yellow light, and acidic pH turns the solution into red.

Due to the pH response of the luciferin reaction, we combine the bioluminescence with the pH modulator as the device readout (Figure 5.4 b). Luciferin and luciferase powders are mixed in the pH 6.7 (measured with a pH meter) Na_2SO_4 and $MgSO_4$ solution inside a PDMS chamber. Cathodic voltage V_c = -0.9 V makes the solution more basic. The optimal condition for the enzyme reaction turns on the bioluminescent light (Figure 5.4 c). When applied to the anodic voltage V_a = 0 V, the solution returns to the original state. Light is off. pH acts as a switch for the light emission reaction.

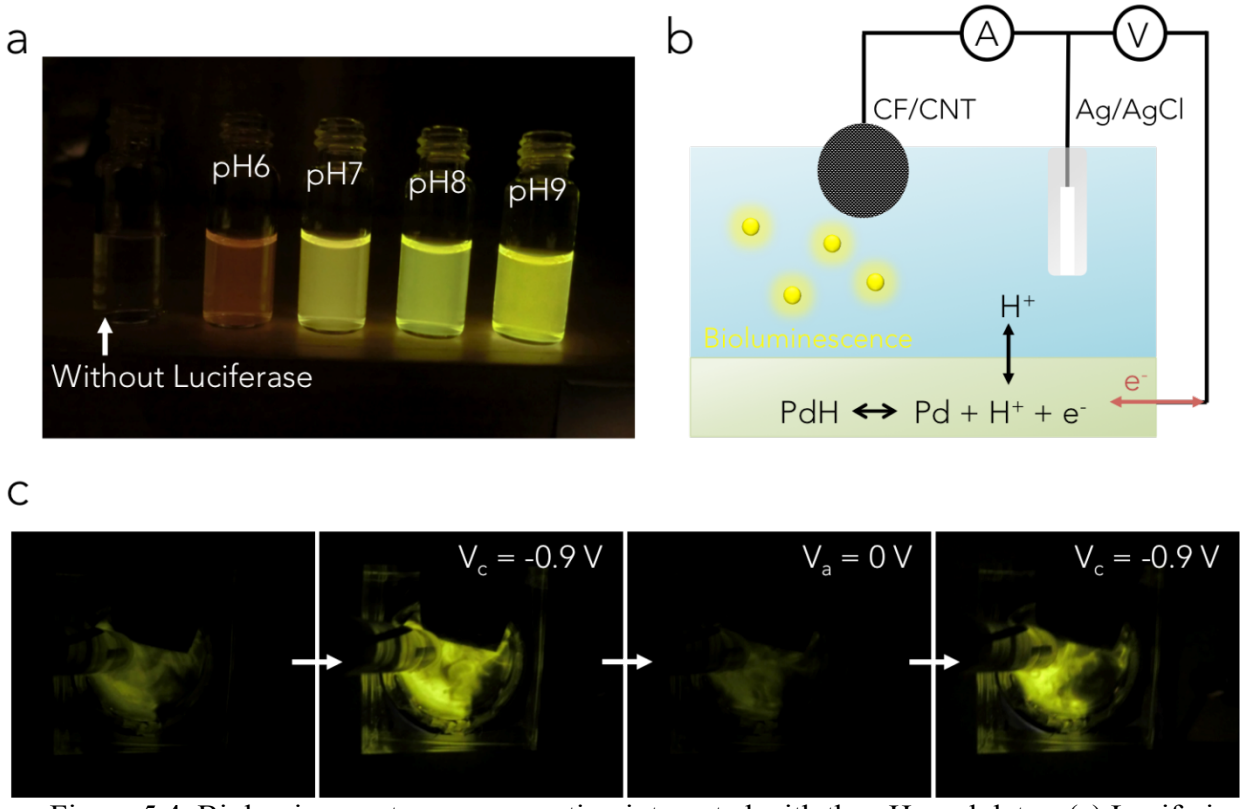

Figure 5.4. Bioluminescent enzyme reaction integrated with the pH modulator. (a) Luciferin and luciferase reaction gives off different color at different pH; (b) Schematic of luciferase enzymatic reaction incorporated in the pH modulator; (c) pH modulation mimics firefly blinking in solution.

The change from Pd to PdH_x increases the solution pH. In order to see a pH decrease, the contact needs to inject H^+ into the solution. I need to start the injection process with PdH_x as the contact. PdH_x-Nafion two-terminal device described in Chapter 2.4 has Nafion as the proton conducting channel. I connected two pH control chambers together with Nafion (Figure 5.5 a). When one contact is loaded with H (I_L in Figure 5.5 b), the potential difference between the contacts transfers H from PdH_x into Pd (I_T in Figure 5.5 b). Then V_a is applied to the second chamber, injecting H^+ from the contact into the solution (I_D in Figure 5.5 b). Using the H^+ circuit, creating an acidic condition is possible. Bioluminescence is integrated as an indication for pH change in both chambers (Figure 5.5 c). As we can see, after the V_a = 0.6 V the left chamber turns from yellow into red.

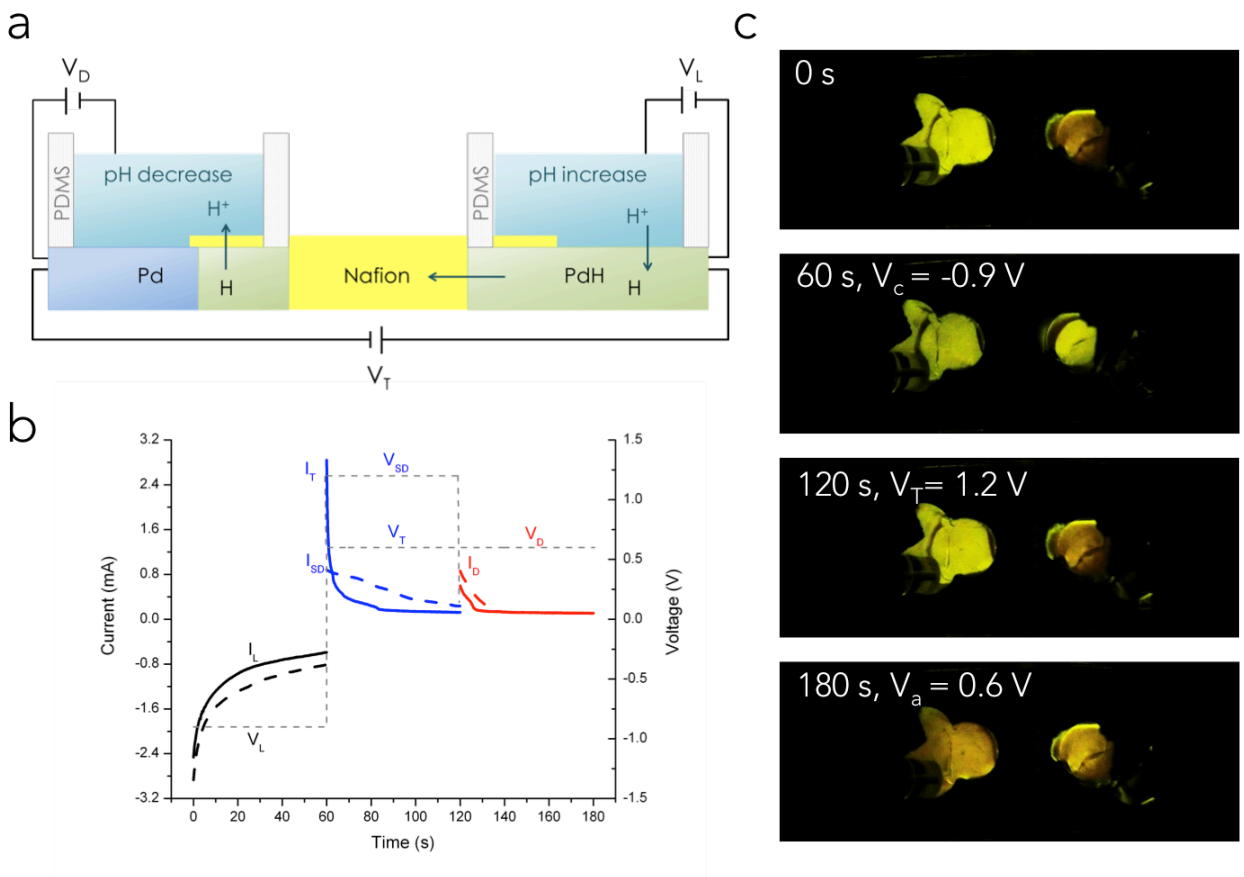

Figure 5.5. Protonic circuit. (a) Schematic of protonic circuit and bioluminescence read-out of pH change; (b) Characteristics of protonic circuit; (c) Bioluminescence show pH change from the pH modulator.

5.5 CELL COMPATIBILITY TEST

After demonstrating H^+ injection into solution, I want to integrate the device with neuron cells and look at the acidosis effect on cell function. The cell interfacing study is done with the collaboration with Dr. Róisín Owens groups in the Department of Bioelectronics (BEL), Center of Microelectronics in Provence, École des Mines de Saint-Étienne. Dr. Owens's group specializes in interfacing artificial devices with biological environment. They have modified ion conducting polymer for cell adhesion,[102] and developed organic electrochemical transistors for biomolecule sensing.[35, 103, 104] Their group has built up abundant techniques and experiences in conducting polymer based biocompatible devices. Among all their exciting results, the ion conducting polymer PEDOT:PSS based microelectrode arrays (MEA) , developed in BEL, have been applied to measure the electrical activity of CA1 pyramidal neurons from a rat hippocampal slice.[30, 105] This device demonstrated the possibility of incorporating ion conducting polymer with MEAs for neuron cell characterization.

To test the cell compatibility of the pH modulator, we start the PC12 cell culture on Nafion surface. PC12 can form dendrite networks on the substrate similar as neurons. Different from neurons, they are not electrogenic cells. Comparatively they are easier to grow. Nafion solution is spun-coated on the substrate. The substrates are immersed in collagen IV solution overnight to create an adhesive layer for cell attachment. Then PC12 cells are seeded, cultured, and monitored their growth at different time period (Figure 5.6). After 6 days of cell culture, a nice cell dendrite network is formed on Nafion surface.

Due to the limited time, I didn't have enough time to finish the cell interfacing work. However, the excellent Nafion cell compatibility shows a promising start. Future work includes downscaling of the pH controlling devices to be compatible with cell detection; neuronal cell culture; the effect of local pH change on neuronal cell functions.

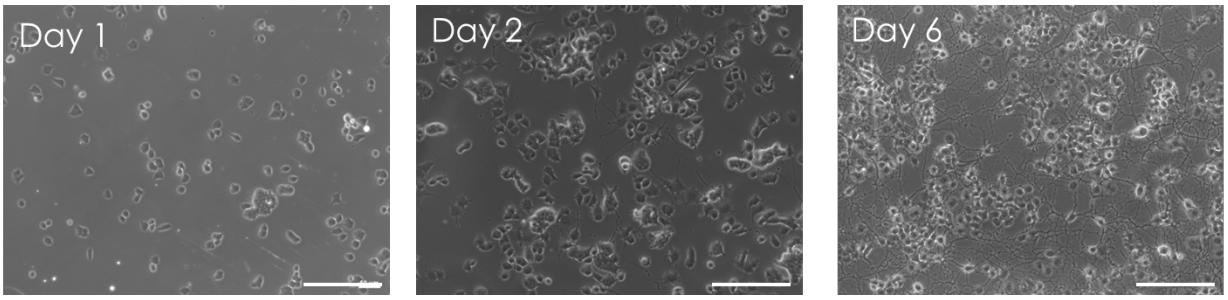

Figure 5.6. Nafion cell compatibility test. Scale bar: 150 μm.

5.6 CONCLUSION

PdH_x contact can control H^+ transfer in solution with an electrochemical setup. H^+ transfer between the contact and solution depends on the protochemical potential of the system. The pH of the solution (the H^+ strength) affects the PdH_x formation, reflecting as different threshold V_c, and PdH_x depletion, showing as different V_a. Measuring I_c and I_a can monitor the cathodic and anodic reactions on the Pd WE as well. A high capacitance CE stores the H^+ in solution, which changes the solution pH. The pH modulating process can affect the pH sensitive firefly bioluminescence lighting. The protonic device finally tested for cell compatibility, paving the way for integrating the device with biological systems in the future.

Chapter 6. FUTURE OUTLOOK

Bioprotonic devices communicate between traditional electronics (electrons as charge carriers) and biological systems (protons as charge carriers). Being able to control H^+ flow with artificial devices offers the possibilities to mimic a natural ion flow process and to modulate biological functions. Therefore the protonic devices can act in close proximity to the biotic-abiotic transducer interface.

Finding a proton transparent contact is essential for the H^+ conducting devices. After absorption of hydrogen atoms, Pd expands in volume up to about 10%, which increases the possibilities of metal fracture so as to limit the life span of the contact. Looking for a H^+ injecting polymer counterpart, such as highly doped acidic or basic polymers, may broaden the applications of H^+ conducting devices. Flexible polymer contacts may avoid cracking problems and have better contact with the biological systems. In terms of proton conducting materials, improved synthetic techniques that are able to control the degree of substitution of functional groups may be able to control the H^+ conductivity of the material, similar as controlling doping concentration in semiconductors. Temperature dependent conductivity study may reinforce the semiconductor similarities of such protonic devices.

BIBLIOGRAPHY

[1] T. Nishi, M. Forgac, Nat Rev Mol Cell Bio 2002, 3, 94.
[2] J. A. Wemmie, M. P. Price, M. J. Welsh, Trends Neurosci 2006, 29, 578.
[3] J. Y. Du, L. R. Reznikov, M. P. Price, X. M. Zha, Y. Lu, T. O. Moninger, J. A. Wemmie, M. J. Welsh, P Natl Acad Sci USA 2014, 111, 8961.
[4] B. Hille, *Ion Channels of Excitable Membranes*, Vol. 1, Sinauer Associates Inc., 2001.
[5] P. Mitchell, Nature 1961, 191, 144.
[6] J. M. Walter, D. Greenfield, C. Bustamante, J. Liphardt, P Natl Acad Sci USA 2007, 104, 2408.
[7] S. Cukierman, Biochimica et biophysica acta 2006, 1757, 876.
[8] J. F. Nagle, M. Mille, H. J. Morowitz, J Chem Phys 1980, 72, 3959.
[9] L. Glasser, Chem Rev 1975, 75, 21.
[10] M. Eigen, L. Demaeyer, Proc R Soc Lon Ser-A 1958, 247, 505.
[11] Bardelme.Gh, Biopolymers 1973, 12, 2289.
[12] E. J. Murphy, J Colloid Interf Sci 1976, 54, 400.
[13] R. Pomes, B. Roux, Biophys J 2002, 82, 2304.
[14] T. E. DeCoursey, J. Hosler, Journal of the Royal Society Interface 2014, 11.
[15] S. K. Dishari, M. A. Hickner, Macromolecules 2013, 46, 413.
[16] Y. Sone, P. Ekdunge, D. Simonsson, J Electrochem Soc 1996, 143, 1254.
[17] A. O. a. C. G. Gerald Pourcelly, J. Electroanal. Chem 1990, 287, 17.
[18] J. Volkmann, A. Albanese, A. Antonini, K. R. Chaudhuri, C. E. Clarke, R. M. A. de Bie, G. Deuschl, K. Eggert, J. L. Houeto, J. Kulisevsky, D. Nyholm, P. Odin, K. Ostergaard, W. Poewe, P. Pollak, J. M. Rabey, O. Rascol, E. Ruzicka, M. Samuel, H. Speelman, O. Sydow, F. Valldeoriola, C. van der Linden, W. Oertel, J Neurol 2013, 260, 2701.
[19] A. Noy, Adv Mater 2011, 23, 807.
[20] F. Patolsky, B. P. Timko, G. F. Zheng, C. M. Lieber, Mrs Bull 2007, 32, 142.
[21] S.-C. J. Huang, A. B. Artyukhin, N. Misra, J. A. Martinez, P. A. Stroeve, C. P. Grigoropoulos, J.-W. W. Ju, A. Noy, Nano Lett 2010, 10, 1812.
[22] M. D. Angione, S. Cotrone, M. Magliulo, A. Mallardi, D. Altamura, C. Giannini, N. Cioffi, L. Sabbatini, E. Fratini, P. Baglioni, G. Scamarcio, G. Palazzo, L. Torsi, P Natl Acad Sci USA 2012, 109, 6429.
[23] F. Patolsky, G. F. Zheng, O. Hayden, M. Lakadamyali, X. W. Zhuang, C. M. Lieber, P Natl Acad Sci USA 2004, 101, 14017.
[24] Z. Jiang, Q. Qing, P. Xie, R. X. Gao, C. M. Lieber, Nano Lett 2012, 12, 1711.
[25] F. Patolsky, B. P. Timko, G. H. Yu, Y. Fang, A. B. Greytak, G. F. Zheng, C. M. Lieber, Science 2006, 313, 1100.
[26] S. H. Jo, T. Chang, I. Ebong, B. B. Bhadviya, P. Mazumder, W. Lu, Nano Lett 2010, 10, 1297.
[27] K. Kim, C. L. Chen, Q. Truong, A. M. Shen, Y. Chen, Adv Mater 2013, 25, 1693.
[28] R. M. Owens, G. G. Malliaras, Mrs Bull 2010, 35, 449.
[29] L. Kergoat, B. Piro, M. Berggren, M. C. Pham, A. Yassar, G. Horowitz, Org Electron 2012, 13, 1.
[30] D. Khodagholy, T. Doublet, P. Quilichini, M. Gurfinkel, P. Leleux, A. Ghestem, E. Ismailova, T. Herve, S. Sanaur, C. Bernard, G. G. Malliaras, Nat Commun 2013, 4.

[31] M. Berggren, J. Isaksson, P. Kjall, D. Nilsson, N. D. Robinson, A. Richter-Dahlfors, Nature Materials 2007, 6, 673.
[32] D. T. Simon, S. Kurup, K. C. Larsson, R. Hori, K. Tybrandt, M. Goiny, E. H. Jager, M. Berggren, B. Canlon, A. Richter-Dahlfors, Nature Materials 2009, 8, 742.
[33] K. Tybrandt, R. Forchheimer, M. Berggren, Nat Commun 2012, 3.
[34] L. H. J. Scherrine Tria, Adel Hama, Manuelle Bongo and Róisín M. Owens Biosensors 2013, 3, 14.
[35] S. Y. Yang, F. Cicoira, R. Byrne, F. Benito-Lopez, D. Diamond, R. M. Owens, G. G. Malliaras, Chem Commun 2010, 46, 7972.
[36] K. Tybrandt, E. O. Gabrielsson, M. Berggren, J Am Chem Soc 2011, null.
[37] T. Shedlovsky, Science 1951, 113, 2.
[38] T. B. Flanagan, F. A. Lewis, T Faraday Soc 1959, 55, 1409.
[39] C. Gabrielli, P. P. Grand, A. Lasia, H. Perrot, J Electrochem Soc 2004, 151, A1925.
[40] C. Gabrielli, P. P. Grand, A. Lasia, H. Perrot, J Electrochem Soc 2004, 151, A1937.
[41] C. Langhammer, I. Zoric, B. Kasemo, Nano Lett 2007, 7, 3122.
[42] D. Teschner, Z. Revay, J. Borsodi, M. Havecker, A. Knop-Gericke, R. Schlogl, D. Milroy, S. D. Jackson, D. Torres, P. Sautet, Angew Chem Int Edit 2008, 47, 9274.
[43] T. B. Flanagan, F. A. Lewis, J Chem Phys 1958, 29, 1417.
[44] M. J. Vasile, C. G. Enke, J Electrochem Soc 1965, 112, 865.
[45] H. Morgan, R. Pethig, G. T. Stevens, J Phys E Sci Instrum 1986, 19, 80.
[46] A. G. Knapton, Platinum Metals Review 1977, 21, 7.
[47] C. Zhong, J. Wu, C. A. Reinhart-King, C. C. Chu, Acta Biomater 2010, 6, 3908.
[48] T. H. Yang, S. Pyun, Y. Yoon, Electrochim Acta 1997, 42, 1701.
[49] E. E. Josberger, Y. Deng, W. Sun, R. Kautz, M. Rolandi, Adv Mater 2014, n/a.
[50] C. Zhong, Y. Deng, A. F. Roudsari, A. Kapetanovic, M. P. Anantram, M. Rolandi, Nat Commun 2011, 2, 476.
[51] Y. Deng, E. Josberger, J. Jin, A. F. Rousdari, B. A. Helms, C. Zhong, M. P. Anantram, M. Rolandi, Sci. Rep. 2013, 3, 2481.
[52] H. J. Koo, J. H. So, M. D. Dickey, O. D. Velev, Advanced Materials 2011, 23, 3559.
[53] J. W. Hanneken, Vol. Ph.D., Rice University, Houston, Texas 1978.
[54] R. Waser, M. Aono, Nature Materials 2007, 6, 833.
[55] D. B. Strukov, G. S. Snider, D. R. Stewart, R. S. Williams, Nature 2009, 459.
[56] M. Di Ventra, Y. V. Pershin, L. O. Chua, P Ieee 2009, 97, 1717.
[57] B. Eisenberg, P Natl Acad Sci USA 2008, 105, 6211.
[58] T. E. DeCoursey, Cellular and Molecular Life Sciences 2008, 65, 2554.
[59] M. A. Reed, C. Zhou, C. J. Muller, T. P. Burgin, J. M. Tour, Science 1997, 278, 252.
[60] H. Song, Y. Kim, Y. H. Jang, H. Jeong, M. A. Reed, T. Lee, Nature 2009, 462, 1039.
[61] A. Javey, J. Guo, Q. Wang, M. Lundstrom, H. J. Dai, Nature 2003, 424, 654.
[62] K. S. Novoselov, A. K. Geim, S. V. Morozov, D. Jiang, Y. Zhang, S. V. Dubonos, I. V. Grigorieva, A. A. Firsov, Science 2004, 306, 666.
[63] V. F. Petrenko, N. Maeno, J Phys-Paris 1987, 48, 115.
[64] Z. G. Chiragwandi, O. Nur, M. Willander, N. Calander, Appl Phys Lett 2003, 83, 5310.
[65] D. B. Strukov, G. S. Snider, D. R. Stewart, R. S. Williams, Nature 2008, 453, 80.
[66] Q. X. Lai, L. Zhang, Z. Y. Li, W. F. Stickle, R. S. Williams, Y. Chen, Adv Mater 2010, 22, 2448.
[67] R. Karnik, R. Fan, M. Yue, D. Y. Li, P. D. Yang, A. Majumdar, Nano Lett 2005, 5, 943.

[68] C. H. Duan, A. Majumdar, Nature Nanotechnology 2010, 5, 848.
[69] K. Bradley, A. Davis, J. C. P. Gabriel, G. Gruner, Nano Lett 2005, 5, 841.
[70] N. Misra, J. A. Martinez, S. C. J. Huang, Y. M. Wang, P. Stroeve, C. P. Grigoropoulos, A. Noy, P Natl Acad Sci USA 2009, 106, 13780.
[71] N. A. Kotov, J. O. Winter, I. P. Clements, E. Jan, B. P. Timko, S. Campidelli, S. Pathak, A. Mazzatenta, C. M. Lieber, M. Prato, R. V. Bellamkonda, G. A. Silva, N. W. S. Kam, F. Patolsky, L. Ballerini, Adv Mater 2009, 21, 3970.
[72] K. Tybrandt, K. C. Larsson, A. Richter-Dahlfors, M. Berggren, Proceedings of the National Academy of Sciences 2010, 107, 9929.
[73] K. Tybrandt, E. O. Gabrielsson, M. Berggren, J Am Chem Soc 2011, 133, 10141.
[74] L. Y. Chen, Z. G. Tian, Y. M. Du, Biomaterials 2004, 25, 3725.
[75] H. Kayser, F. Rodriguez-Ropero, W. Leitner, M. Fioroni, P. D. de Maria, Rsc Adv 2013, 3, 9273.
[76] A. B. Mostert, B. J. Powell, F. L. Pratt, G. R. Hanson, T. Sarna, I. R. Gentle, P. Meredith, P Natl Acad Sci USA 2012, 109, 8943.
[77] A. Richter-Dahlfors, K. Svennersten, K. C. Larsson, M. Berggren, Bba-Gen Subjects 2011, 1810, 276.
[78] K. H. Kim, S. Gaba, D. Wheeler, J. M. Cruz-Albrecht, T. Hussain, N. Srinivasa, W. Lu, Nano Lett 2012, 12, 389.
[79] L. Xu, Z. Jiang, Q. Qing, L. Mai, Q. Zhang, C. M. Lieber, Nano Lett 2012.
[80] C. Zhong, A. Cooper, A. Kapetanovic, Z. H. Fang, M. Q. Zhang, M. Rolandi, Soft Matter 2010, 6, 5298.
[81] R. Riva, H. Ragelle, A. des Rieux, N. Duhem, C. Jerome, V. Preat, Adv Polym Sci 2011, 244, 19.
[82] Y. Shigemasa, H. Matsuura, H. Sashiwa, H. Saimoto, International Journal of Biological Macromolecules 1996, 18, 237.
[83] V. M. Volgin, A. D. Davydov, J Membrane Sci 2005, 259, 110.
[84] S. M. Sze, Cc/Eng Tech Appl Sci 1982, 28.
[85] S. Cukierman, Bba-Bioenergetics 2006, 1757, 876.
[86] H. J. Morowitz, Am J Physiol 1978, 235, R99.
[87] H. Kawasaki, S. Eguchi, S. Miyashita, S. Chan, K. Hirai, N. Hobara, A. Yokomizo, H. Fujiwara, Y. Zamami, T. Koyama, X. Jin, Y. Kitamura, J Pharmacol Exp Ther 2009, 330, 745.
[88] B. R. R. Kai Kaila, *pH and Brain Function*, Wiley Liss US 1998.
[89] M. Chesler, K. Kaila, Trends Neurosci 1992, 15, 396.
[90] H. Caspers, Speckman.Ej, Epilepsia 1972, 13, 699.
[91] L. Velisek, J. P. Dreier, P. K. Stanton, U. Heinemann, S. L. Moshe, Exp Brain Res 1994, 101, 44.
[92] S. Javaheri, A. Dehemptinne, B. Vanheel, I. Leusen, J Appl Physiol 1983, 55, 1849.
[93] J. Santo-Domingo, N. Demaurex, J Gen Physiol 2012, 139, 415.
[94] T. Miyake, E. E. Josberger, S. Keene, Y. Deng, M. Rolandi, APL Materials 2015, 3.
[95] T. Imokawa, K. J. Williams, G. Denuault, Anal Chem 2006, 78, 265.
[96] E. E. Josberger, Y. X. Deng, W. Sun, R. Kautz, M. Rolandi, Adv Mater 2014, 26, 4986.
[97] J. A. Abys, in *Modern Electroplating*, (Ed: M. P. Mordechay Schlesinger), Wiley, Hoboken, NJ 2010, 327.
[98] P. Simon, Y. Gogotsi, Nature Materials 2008, 7, 845.

[99] K. Haneda, S. Yoshino, T. Ofuji, T. Miyake, M. Nishizawa, Electrochim Acta 2012, 82, 175.
[100] E. Shapiro, C. Lu, F. Baneyx, Protein Eng Des Sel 2005, 18, 581.
[101] S. M. Smith, D. Morgan, B. Musset, V. V. Cherny, A. R. Place, J. W. Hastings, T. E. Decoursey, Proc Natl Acad Sci U S A 2011, 108, 18162.
[102] M. Bongo, O. Winther-Jensen, S. Himmelberger, X. Strakosas, M. Ramuz, A. Hama, E. Stavrinidou, G. G. Malliaras, A. Salleo, B. Winther-Jensen, R. M. Owens, Journal of Materials Chemistry B 2013, 1, 3860.
[103] N. Y. Shim, D. A. Bernards, D. J. Macaya, J. A. DeFranco, M. Nikolou, R. M. Owens, G. G. Malliaras, Sensors-Basel 2009, 9, 9896.
[104] D. Khodagholy, V. F. Curto, K. J. Fraser, M. Gurfinkel, R. Byrne, D. Diamond, G. G. Malliaras, F. Benito-Lopez, R. M. Owens, J Mater Chem 2012, 22, 4440.
[105] M. Sessolo, D. Khodagholy, J. Rivnay, F. Maddalena, M. Gleyzes, E. Steidl, B. Buisson, G. G. Malliaras, Adv Mater 2013, 25, 2135.

VITA

Yingxin Deng was born in Guiyang, China. She graduated from Guiyang No.1 High School in 2006, and graduated with a B.S. in Biomedical Engineering from Sichuan University. She came to the University of Washington in 2010. She received a M.S. in Materials Science and Engineering from the University of Washington in 2012, and a Ph.D. in Materials Science and Engineering from the University of Washington in 2015.